The Astrophysical Journal Supplement Series, 271:61 (16pp), 2024 April https://doi.org/10.3847/1538-4365/ad2a42


# Quasar Winds Caught on Acceleration and Deceleration

Weimin Yi[1], P. B. Hall[2], Zunli Yuan[3], W. N. Brandt[4,5], D. P. Schneider[4,5], Zhicheng He[6], Jin-Ming Bai[1], and Xue-Bing Wu[7,8]
[1] Yunnan Observatories, Kunming, 650216, People's Republic of China; ywm@ynao.ac.cn
[2] Department of Physics and Astronomy, York University, Toronto, ON, M3J 1P3, Canada
[3] Department of Physics, School of Physics and Electronics, Hunan Normal University, Changsha 410081, People's Republic of China
[4] Department of Astronomy & Astrophysics, The Pennsylvania State University, 525 Davey Lab, University Park, PA 16802, USA
[5] Institute for Gravitation and the Cosmos, The Pennsylvania State University, University Park, PA 16802, USA
[6] CAS Key Laboratory for Research in Galaxies and Cosmology, Department of Astronomy, University of Science and Technology of China, Hefei, Anhui 230026, People's Republic of China
[7] Kavli Institute for Astronomy and Astrophysics, Peking University, Beijing 100871, People's Republic of China
[8] Department of Astronomy, Peking University, Yi He Yuan Lu 5, Hai Dian District, Beijing 100871, People's Republic of China
*Received 2023 December 1; revised 2024 February 8; accepted 2024 February 14; published 2024 April 10*

## Abstract

We present an observational study of wind acceleration based on four low-ionization broad absorption line (BAL) quasars (J0136, J1238, J1259, and J1344). J0136 and J1344 (group 1) are radio-quiet and show large BAL-velocity shifts as opposed to stable line-locking associated absorption lines (AALs). Notably, J1344 displays a linear relation between BAL-velocity shift and time interval over three consecutive epochs, characteristic of compelling evidence for BAL acceleration. J1238 and J1259 (group 2) exhibit small BAL-velocity shifts along with steep-spectrum, weak radio emission at 3.0 and 1.4 GHz. All four quasars have spectral energy distributions (SEDs) with a peak at $\lambda_{\rm rest} \sim 10\,\mu$m, suggesting a link between the BAL acceleration and hot dust emission. The group-2 quasars are redder than group-1 quasars and have a steeper rise at $1\,\mu{\rm m} < \lambda_{\rm rest} < 3\,\mu$m in their SEDs. All but J1238 exhibit a steep rise followed by a plateau-like time evolution in BAL-velocity shift. Our investigations, combined with previous studies of BAL acceleration, indicate that (1) the coupling process between the BALs and the interstellar medium (ISM) is one of the major avenues for the origin of quasar reddening and patchy obscuration, (2) AAL outflows are ubiquitous and likely signify large-scale remnants of BAL winds coupled to the ISM, and (3) wind deceleration that is closely linked to the BAL–ISM coupling process may produce weak radio emission in otherwise radio-quiet quasars.

*Unified Astronomy Thesaurus concepts:* Active galactic nuclei (16); Interstellar medium (847); Broad-absorption line quasar (183)

## 1. Introduction

Broad absorption line (BAL; Weymann et al. 1991) features imprinted on quasar spectra are unambiguous evidence for intrinsic outflows, whose kinetic power could be sufficient for triggering active galactic nuclear feedback and hence could control the growth of supermassive black holes (SMBHs; Fabian 2012). BAL winds are believed to be launched from accretion disks that have a typical size of ∼0.01 pc if driven by an SMBH with $\sim 10^9\ M_\odot$ (Murray et al. 1995; Proga et al. 2000). Observationally, however, many studies suggest that the vast majority of BAL winds are likely to be located at a range of ∼1–1000 pc from their SMBHs (e.g., Capellupo et al. 2011; McGraw et al. 2017; Arav et al. 2018; He et al. 2019). Therefore, probing the inner physics of BAL winds, such as the acceleration mechanisms and the impact on the interstellar medium (ISM), has become a topic of increasing interest.

BAL quasars are divided into two major classes, namely high-ionization BAL (HiBAL) and low-ionization BAL (LoBAL) quasars (e.g., Weymann et al. 1991; Trump et al. 2006). A bona fide BAL is characterized by an absorption trough, whose width is broader than $2000\,{\rm km\,s^{-1}}$ under 90% of the continuum level with a minimum line-of-sight (LOS) velocity of $>3000\,{\rm km\,s^{-1}}$ (Weymann et al. 1991). To form such remarkable absorption features, acceleration of BAL winds must somehow play a role during the lifetime of BAL quasars. Grier et al. (2016) conducted the first systematic investigation of BAL acceleration, from which they found only two out of 140 quasars showing solid evidence of BAL acceleration. Such a low incidence (∼1.43%) of BAL acceleration is likely underestimated since their work is based on the search for monolithic velocity shifts across the entire BAL trough over multiple spectroscopic epochs. Nevertheless, one would expect from a sample of ∼100,000 BAL quasars (Lyke et al. 2020) that a fairly large number of objects could be caught on BAL acceleration even with an incidence of ∼1.43%.

Hall et al. (2007) reported one of the first cases of a quasar exhibiting BAL-acceleration signatures, whose average acceleration has a magnitude consistent with that estimated from a longer sampling interval in a subsequent study (Byun et al. 2022), although more data are needed before drawing a firm conclusion of BAL acceleration. This point is particularly true when noticing the "jerk" phenomenon of BAL acceleration; that is, the change in acceleration with time (e.g., Capellupo et al. 2011; Filiz et al. 2013; Grier et al. 2016; Rogerson et al. 2016). For example, Rogerson et al. (2016) identified a quasar showing the emergence of BALs at two widely separated velocities. Specifically, trough A showed a fluctuating velocity centroid due to variability of the trough profile; however, trough B showed an increasing outflow velocity over three

epochs, which, if confirmed to be acceleration, would represent rest-frame 16 and 55 cm $s^{-2}$ between the first and second and the second and third epochs, respectively. Simple radiative acceleration models can match such values at small radii (see their Section 4.1.2), but would have to invoke strong variability of the ionizing continuum to explain such large changes in acceleration. Similarly, Aromal et al. (2021) reported a quasar having two distinct BAL troughs, one of which is consistent with BAL acceleration along with variability in rest equivalent width (REW) while the other exhibits complex variations in profile. Recently, Xu et al. (2020) argued for the largest BAL acceleration detected in a quasar, despite having spectra from only two sampling epochs. Perhaps a more ambiguous example for acceleration is NGC 3783, a local active galactic nucleus that has been extensively studied from nearly two decades of high-spectral-resolution observations, for which Gabel et al. (2003) proposed an explanation of radial deceleration; however, this argument appears to be increasingly uncertain in later studies (e.g., Scott et al. 2014; Kriss et al. 2019).

Another major difficulty for the analysis of BAL phenomena is the prevalence of BAL-profile variability among BAL quasars. As introduced above, time variability has become a widely used tool for probing the formation, acceleration, and evolution of BAL winds, due primarily to the fact that the vast majority of quasars and their host galaxies cannot be spatially resolved by current instruments. Generally, well-separated, multiepoch spectroscopy is a powerful technique for identifying genuine cases of BAL acceleration and for placing valuable constraints on the BAL physics, lifetime, and location (e.g., Aromal et al. 2021; Yi et al. 2022). In reality, however, BAL acceleration and BAL-profile variability may occur simultaneously, making a firm identification of BAL acceleration difficult or sometimes impossible, even with the aid of long-term, high-quality, and high-cadence sampling spectra (e.g., Kriss et al. 2019; Yi & Timlin 2021; Byun et al. 2022). This situation can be easily understood given the complex nature of BAL winds, which are typically characterized by many subflows that are independent of each other and vary stochastically. Regarding the analysis of BAL acceleration, another three facts must be taken into account. First, the majority of BAL quasars have not been spectroscopically observed more than three times, rendering any attempts at identifying genuine acceleration difficult. Second, BALs may be transient during the spectroscopic monitoring time. Third, the decomposition of a complex, seemingly single BAL trough is notoriously difficult due to blending and/or partial covering along our LOS. Nevertheless, genuine BAL acceleration or deceleration events may provide unique insights into the origin of quasar reddening and weak radio emission, an interesting yet open question invoked by recent studies (e.g., Klindt et al. 2019; Calistro Rivera et al. 2021).

In this work, we conduct a systematic analysis of BAL acceleration from the LoBAL variability sample in Yi et al. (2019) and the HiBAL acceleration sample in Grier et al. (2016), from which we identified four BAL-acceleration quasars. The first two (and in one case four) epochs of spectroscopic observations of the four quasars were performed in various phases of the Sloan Digital Sky Survey (SDSS; York et al. 2000; Eisenstein et al. 2011; Blanton et al. 2017) and were accessed from the SDSS public database. Additional observations were obtained with a variety of other facilities (see Section 2.2). The new data were designed to systematically investigate LoBAL acceleration and to bridge the gap over HiBAL acceleration. We emphasize that (1) all time intervals are in the quasar rest frame; (2) the term "acceleration" refers to either actual acceleration or deceleration unless stated otherwise; (3) velocity or kinematic shift, by definition, is a relative quantity and does not depend on the accuracy of systemic redshift; and (4) zero velocity is converted by the shorter-wavelength component of each doublet at systemic redshift throughout this work.

## 2. Observations and Data Reduction

### 2.1. Candidate Selection

We began with the selection of BAL-acceleration candidates from the LoBAL-variability sample in Yi et al. (2019), where a few quasars were found to show apparent velocity shifts within the sampling epochs. Following Grier et al. (2016), we first searched for quasar candidates of BAL acceleration from Yi et al. (2019) by requiring monolithic velocity shifts in BAL profile over at least three spectroscopic epochs for each quasar. However, none of the quasars from that work satisfy the requirement, probably because (1) the majority of quasars from Yi et al. (2019) have been observed only twice, (2) the occurrence of BAL acceleration is intrinsically rare, (3) BAL-profile changes are ubiquitous as reported in previous studies, and/or (4) it is impossible to assess BAL acceleration from BAL-transient events without sufficient sampling epochs before its disappearance.

Unfortunately, we did not find any quasars with spectra from three or more different epochs from Yi et al. (2019) that displayed monolithic BAL shifts, i.e., they often exhibit large BAL-profile changes and pose great challenges to ascertaining the origin of their BAL variability. Therefore, we then searched for monolithic velocity shifts among these quasars that have spectra from only two different epochs and found three candidates, namely SDSS J134444.32 + 315007.6, SDSS J123820.19 + 175039.1, and SDSS J125942.79 + 121312.6 (hereafter J1344, J1238, and J1259) meeting the requirement. We also add the strongest BAL-acceleration candidate, namely SDSS J013656.31−004623.8 (hereafter J0136), from Grier et al. (2016) to our final BAL-acceleration list, due partly to the presence of LoBAL species, which was mentioned only in passing in that work.

The early-epoch spectra of the four BAL-acceleration candidates are retrieved directly from the SDSS DR16 archive (see Lyke et al. 2020); in addition, we also quantify the variability in both the Mg II BAL and continuum shape for J0136 following the same prescription as in Yi & Timlin (2021). Interestingly, like the six quasars reported in Yi & Timlin (2021), J0136 is also undergoing a LoBAL → HiBAL transformation along with a decrease in dust; in stark contrast, the other three BAL-acceleration candidates, which have small fractional REW changes, become redder in later epochs. Below we illustrate them in detail with the aid of archived multi-wavelength photometry and new spectroscopic observations.

### 2.2. New Observations

To facilitate the assessment of BAL acceleration, we placed these objects in the target list of our spectroscopic monitoring campaign of subsequent BAL variability for individual quasars of interest. We obtained additional optical spectra for these quasars using the Low-Resolution Spectrograph-2 (LRS-2;

Chonis et al. 2014) mounted on the Hobby–Eberly Telescope (HET; Ramsey et al. 1998). These newly obtained spectroscopic data were processed with the LRS-2 pipeline,[9] which incorporates an improved procedure for flux calibration with a typical uncertainty of ∼15% (Hill et al. 2021). Long-slit (2.″5 in width) spectra were mainly acquired by the Yunnan Faint Object Spectrograph and Camera (YFOSC) mounted on the Lijiang 2.4 m Telescope (LJT; Fan et al. 2015; Wang et al. 2019). We also obtained another long-slit (1.″0 in width) spectrum for the faintest quasar, J1259, using the multiobject double spectrographs (MODS) mounted on the Large Binocular Telescope (LBT), which covers a wide wavelength range of 0.33–1.03 $\mu$m. These long-slit data were processed using standard IRAF routines, including bias subtraction, flat-field correction, cosmic-ray removal, spectral extraction, wavelength identification, and flux calibration.

Near-IR spectroscopic observations were performed with the TripleSpec spectrograph at the Palomar Hale 200 inch telescope (P200/TripleSpec; Wilson et al. 2004) for J0136 and J1238. TripleSpec provides a wide wavelength coverage (0.95–2.46 $\mu$m) at an average spectral resolution of ∼2700, allowing simultaneous observations in the $J/H/K$ bands. A slit width of one arcsecond and the ABBA dither pattern along the slit were chosen to improve the sky subtraction during the observations. We carefully examined the data quality flags and wavelength calibration in each epoch for each quasar, and did not find significant instrumental artifacts from the spectral regions of interest.

The log of observations is summarized in Table 1 and the multiepoch optical spectra of each candidate are presented in Figure 1 for an overall view.

## 3. Spectral Measurements and Identifications of BAL Acceleration

Following a similar procedure from Yi et al. (2019), we first model the local continuum of interest by fitting a reddened power-law function to the relatively line-free spectral regions identified through visual inspection for each quasar. The BALs and broad emission lines (BELs) are then normalized by the fitted continuum from each epoch for each quasar. Finally, the quantities such as REW are measured by the continuum-normalized spectra over the epochs, which allows us to quantify the BALs and BELs and the related time variability therein for each quasar.

We highlight that the REW alone may fail to quantify BAL variability, especially in cases where BALs show velocity shifts over different epochs but lack significant changes in their profiles, leading to an approximately equal REW for the two BALs chosen from two different epochs. This issue must be addressed before performing a further analysis of BAL acceleration, given that one would naturally expect to see velocity shifts of the BAL over multiple epochs from BAL-acceleration candidates. Therefore, it is mandatory to examine the BAL-profile variability in detail and, whenever possible, to identify independent or correlated BAL subflows from epoch to epoch for each quasar. Such an investigation is important given the diversity of BAL-profile variability that may reflect different velocity components in a single BAL trough arising from largely different physical regions (e.g., Arav et al. 2015; Yi et al. 2019; Yi & Timlin 2021). This is also one of the most challenging issues for the analysis of BAL variability.

Ideally, high-resolution spectroscopy with high signal-to-noise ratio (S/N) can provide powerful diagnostics to probe the detailed variability for a given BAL trough, but in reality it is almost impossible to obtain multiepoch, high-resolution spectra for the majority of quasars given their faint apparent magnitudes. We circumvent this challenge by taking advantage of well-separated, intermediate-resolution spectra for each quasar selected. All but the LJT/YFOSC spectra displayed below are smoothed by a 3 pixel boxcar filter (∼200 km s$^{-1}$) for optimal visual inspection unless stated otherwise.

### 3.1. The Criteria of BAL Acceleration

As mentioned in the Introduction, identifications of BAL-acceleration events from apparent velocity shifts are often challenging due to the complex nature of BAL winds. This issue can be alleviated to some extent by placing stringent criteria to select BAL-acceleration candidates (Grier et al. 2016); however, the requirement of a monolithic shift for BAL acceleration in their work, such that the entire BAL trough is clearly shifted but remains generally unchanged in profile, could potentially miss cases of genuine BAL acceleration, given the prevalence of BAL-profile variability on both long and short timescales (e.g., Capellupo et al. 2011; Hemler et al. 2019; Yi et al. 2019). To further mitigate this issue and search for potentially more cases of BAL acceleration, there are three prerequisites: (1) at least three different epochs spanning more than one rest-frame year are required for a quasar, (2) the BAL of interest is similar in profile and has an overlap in velocity from epoch to epoch, and (3) the BAL of interest must be free of strong overlapping absorption produced by different ions. Based upon the above preconditions, we classify tentative, strong, and compelling cases of BAL acceleration using the following criteria.

1. Tentative case: the entire BAL trough of interest is characterized by a monolithic velocity shift, or the same BAL subflow is persistent and shows a velocity shift over multiple epochs.
2. Strong case: the BAL velocity exhibits a monotonic change over at least three consecutive spectroscopic epochs.
3. Compelling case: in addition to criterion 2, the measured velocity shifts follow the same linear relation with time interval.

Following the prescription of Grier et al. (2016), we perform a cross-correlation function (CCF) analysis to measure the monolithic velocity shift between two different epochs for a BAL of interest. Specifically, we run the cross-correlation analysis for each of the 10,000 iterations via a Monte Carlo approach (see the bottom left panel of Figure 2).

Then, we adopt the median of these cross-correlation peaks as the best velocity shift, with an error bar depicting the 90% percentile confidence level. We also performed a similar analysis (Monte Carlo simulations) for the BAL of interest using the reduced $\chi^2_{12}$ (see Yi et al. 2019 for its definition). This exercise found that the velocity shift and uncertainty are in excellent agreement with those derived by the CCF analysis. For simplicity, we adopt the CCF analysis as a standard routine to measure the BAL-velocity shifts and to quantify their

[9] https://github.com/grzeimann/Panacea

**Table 1**
Spectroscopic Observations of the Four BAL-acceleration Quasar Candidates

| Name (Abbreviation) | Instrument | Date (MM-DD-YYYY) | MJD | Exposure Time (s) | $\lambda$ Coverage (Å) | Resolution ($\lambda/\Delta\lambda$) |
|---|---|---|---|---|---|---|
| | SDSS | 10-21-2001 | 52203 | 3106 | 3800–9200 | 1800 |
| J013656.31-004623.8 | SDSS | 09-05-2010 | 55444 | 6305 | 3650–10300 | 1800 |
| (J0136) | SDSS | 12-21-2014 | 57012 | 4500 | 3650–10300 | 1800 |
| $z = 1.7154$ | SDSS | 11-24-2017 | 58081 | 3600 | 3650–10300 | 1800 |
| | HET/LRS-2 | 10-29-2021 | 59516 | 1210 | 3700–6840 | 2500 |
| | P200/TripleSpec | 10-16-2021 | 59503 | 3600 | 10000–25000 | 2700 |
| | SDSS | 05-14-2007 | 54234 | 3406 | 3800–9200 | 1800 |
| J123820.19 + 175039.1 | SDSS | 04-18-2012 | 56035 | 2702 | 3650–10300 | 1800 |
| (J1238) | P200/TripleSpec | 03-05-2018 | 58182 | 900 | 10000–25000 | 2700 |
| $z = 0.453$ | LJT/YFOSC | 03-21-2018 | 58198 | 900 | 3400–9000 | 380 |
| | HET/LRS-2 | 04-02-2021 | 59306 | 480 | 3700–6840 | 2500 |
| | SDSS | 04-13-2005 | 53473 | 3700 | 3800–9200 | 1800 |
| J125942.79 + 121312.6 | SDSS | 02-22-2012 | 55983 | 2702 | 3650–10300 | 1800 |
| (J1259) | HET/LRS-2 | 04-08-2019 | 58216 | 900 | 3700–10300 | 2500 |
| $z = 0.7517$ | LJT/YFOSC | 04-28-2018 | 58601 | 3000 | 3400–9000 | 380 |
| | LBT/MODS | 02-15-2020 | 58894 | 1800 | 3300–10300 | 2200 |
| | HET/LRS-2 | 04-04-2021 | 59308 | 1707 | 6500–10300 | 2500 |
| | SDSS | 05-13-2005 | 53503 | 2700 | 3800–9200 | 1800 |
| J134444.32 + 315007.6 | SDSS | 03-12-2013 | 56363 | 2700 | 3650–10300 | 1800 |
| (J1344) | LJT/YFOSC | 04-16-2018 | 58224 | 1500 | 3400–9000 | 380 |
| $z = 1.44$ | HET/LRS-2 | 01-06-2019 | 58489 | 900 | 3700–6840 | 2500 |
| | HET/LRS-2 | 06-19-2021 | 59384 | 1710 | 3700–6840 | 2500 |

uncertainties. We identified one compelling, one strong, and two tentative cases of BAL acceleration based on the above criteria.

### 3.2. J1344: A Case with Compelling Evidence for BAL Acceleration

J1344 is one of the quasars having two distinct BALs from the sample of Yi et al. (2019); moreover, one of the BALs contains a variable region based on the measurements from the SDSS spectra from two different epochs as recorded in the catalog. A subsequent analysis of this quasar using the two SDSS spectra was performed by Lu & Lin (2020), where they found large velocity shifts traced by both Al III and Mg II for the high-velocity BAL, and hence speculated that it could be associated with actual BAL acceleration. However, as mentioned above, at least three spectroscopic epochs are required to assess the possibility of BAL acceleration in a robust manner. To achieve this goal, we have obtained three additional spectra by using HET/LRS-2 and LJT/YFOSC. Although the YFOSC spectrum at MJD 58224 has a low spectral resolution and S/N, a reliable velocity shift can be measured via the CCF approach; moreover, it is helpful for visual inspection and can be used for flux calibration of the HET/LRS-2 spectrum obtained at MJD 58489, when assuming that there is negligible variability in continuum over such a short time interval. In combination with the well time-separated optical spectra spanning nearly two decades, we can now investigate BAL acceleration in a robust manner for this quasar. One can see from Figure 3 that there are some interesting features from the normalized spectra: (1) the high-velocity BAL-1 and low-velocity BAL-2 are detected in Mg II, Al III, and C IV over the sampling epochs; (2) the BAL-1 profiles are similar over the epochs in either Al III or Mg II except for small changes in trough depth; (3) the BAL-1 velocity increased monotonically from MJD 53503 to 58224 and then appears to level off or perhaps decelerate after that epoch; (4) the Mg II BAL-2 remains unchanged in trough depth over the epochs, despite a large increase in trough width and a slight increase in centroid velocity; (5) a third Al III BAL with $v_{\rm LOS} \sim -11{,}000$ km s$^{-1}$ is significantly detected only at MJD 56363, for which we cannot assess its variability in detail.

Using the spectrum from the first epoch as a benchmark, we separate the five epochs into four time intervals in an ascending order. To measure the velocity shifts in a robust manner, the Mg II BAL-1 that has a higher S/N than the corresponding Al III BAL-1 is treated as the main tracer for the cross-correlation analysis. The measured velocity shifts are $1120^{+70}_{-260}$, $1780^{+360}_{-60}$, $1670^{+200}_{-65}$, and $1650^{+260}_{-130}$ km s$^{-1}$ over the four intervals via this method. Similarly, performing a CCF analysis of the Al III BAL-1 yields $980^{+230}_{-430}$, $1620^{+390}_{-390}$, $1570^{+230}_{-330}$, and $1410^{+400}_{-260}$ km s$^{-1}$ for the four time intervals, respectively (see the MJD versus $\Delta v_{\rm LOS}$ panel in Figure 3). The velocity shifts derived by the two different methods are consistent within the error bars, reinforcing the argument for BAL acceleration. In combination with the same linear relation over the two consecutive time intervals before MJD 58224, we believe that the observations provide compelling evidence for BAL acceleration. On the other hand, by closely examining the Al III BAL-1 profiles, we identified the same subflow with three absorption peaks presumably linked to three different-velocity, blueward components of Al III doublets from the three spectra with relatively high S/N (see left subpanels of Figure 3 for details). This identification is further supported by blueward components of Mg II doublets at the same velocities corresponding to the Al III BAL-1 subflow in each epoch (see the vertical dotted lines in Figure 3), although a smaller velocity split of the doublet in Mg II than in Al III makes it somewhat uncertain. Notably, the velocity shifts traced by the subflow are in excellent agreement with those derived from the entire BAL via the CCF method over the three epochs, reinforcing the argument for acceleration.

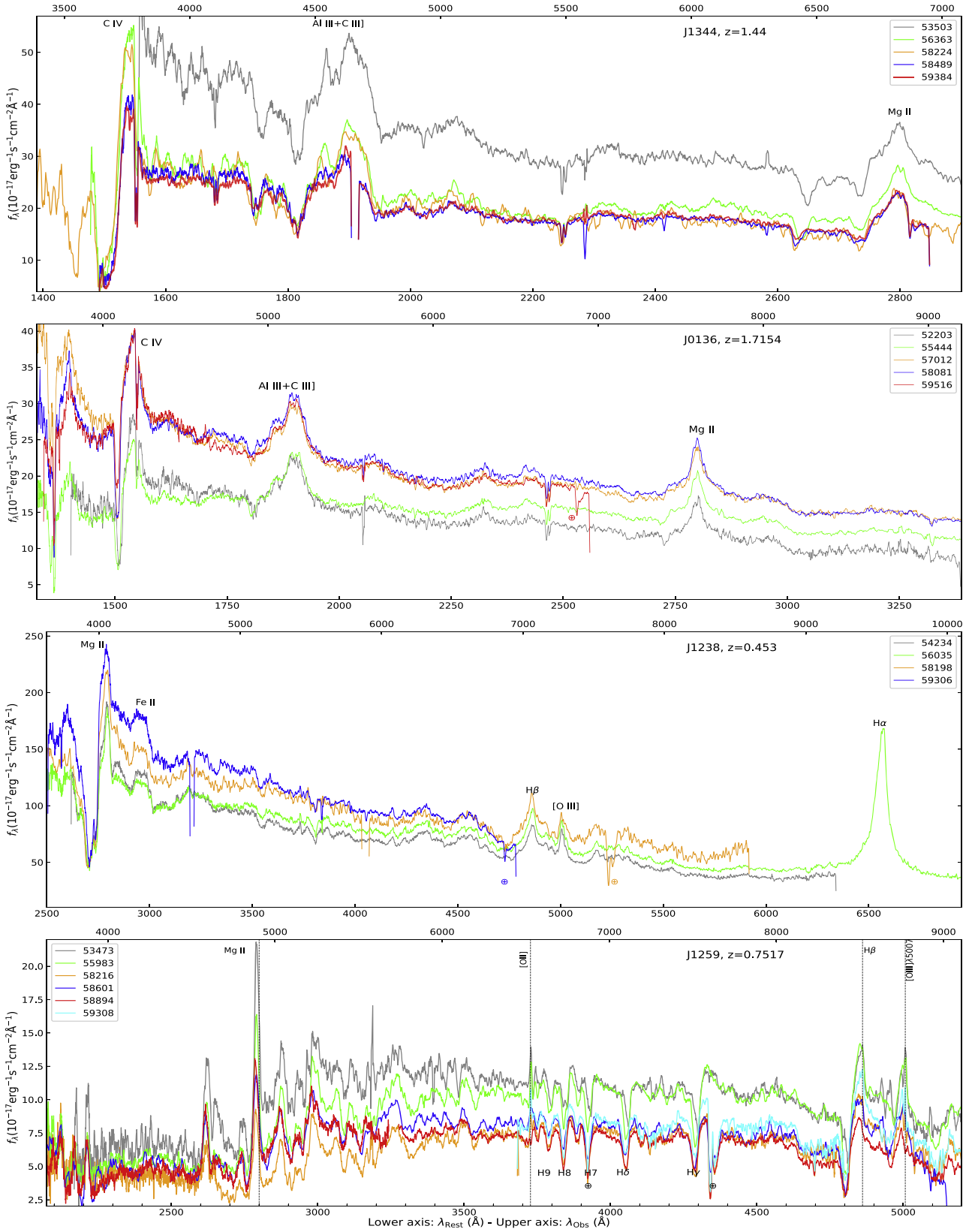


**Figure 1.** Multiepoch optical spectra (smoothed by a 7 pixel boxcar filter corresponding to ∼420 km s$^{-1}$) of the four quasars having signatures of BAL acceleration, in which the spectral fluxes of J1238 and J1259 are recalibrated by *V*-band photometry using the first SDSS epoch as a benchmark. The MJDs of individual observations are given in the upper corner of each panel. Plus symbols mark telluric absorption.

To analyse the variability of BELs, a velocity range of $-2600\,\mathrm{km\,s^{-1}} < v_{\mathrm{LOS}} < 2500\,\mathrm{km\,s^{-1}}$ is chosen to characterize their core-emission features based on visual inspection of the C IV, Al III, and Mg II BELs. Note that Fe II emission contributes only slightly to the core portion of the Mg II BEL. Surprisingly, the Al III BEL nearly disappeared by MJD 59384 while the Mg II

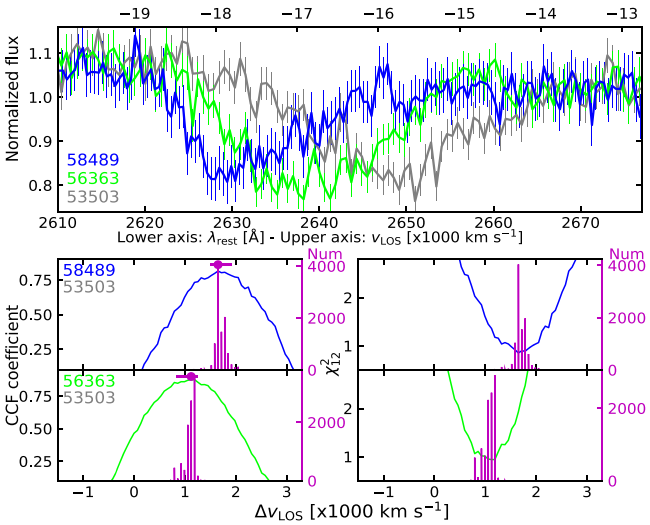


**Figure 2.** Demonstration of monolithic velocity shifts for the Mg II BAL in J1344 over three well-separated epochs (top) via the CCF (bottom left) and $\chi^2_{12}$ (bottom right) analyses, in which the bar histograms correspond to the peaks generated from 10,000 Monte Carlo simulations, with the dot and error bars depicting the median value of the histogram and the 90% percentile confidence level. Both analyses yield a closely similar velocity shift in each time interval.

BEL varied only slightly in fractional REW over the epochs. In addition, the C IV BEL experienced a sharp drop in REW after MJD 58224. Such dramatic variability of the C IV BEL has rarely been reported (Ross et al. 2020).

Regarding the evolution of BALs, it is clear that the BAL-1 and BAL-2 REWs exhibit an overall opposite pattern of time variability after MJD 56363 (see the REW versus MJD panel in Figure 3), which may be related to transverse motions caused by multiple streams moving across our LOS or acceleration /deceleration events (see Section 5). Interestingly, the Al III BAL-1 and BEL become weakened after MJD 56363, while the Al III BAL-2 and BEL show an opposite trend of time variability in REW after MJD 56363 (see the MJD versus REW panel of Figure 3), suggestive of the BEL having a stronger link to BAL-1 in Al III. To provide additional diagnostics for the analysis of the observed BAL/BEL variability, we added a panel of MJD versus $f_{1700}$ (the continuum flux at $\lambda_{\rm rest} = 1700$ Å) to Figure 3 for comparison. Clearly, the time-variability pattern of $f_{1700}$ is opposite to those of the BALs/BELs from MJD 53503 to 56363, such that the BALs/BELs strengthened when the continuum $f_{1700}$ dimmed by a factor of $\sim$2; in addition, the BAL-1 and BELs (in Al III and Mg II) show a similar time-variability trend to that of $f_{1700}$ after MJD 56363. Conversely, $f_{1700}$ and the velocity shift ($\Delta v_{\rm LOS}$) exhibit an opposite time-variability pattern before MJD 58224; in addition, BAL-1 and BAL-2 show an opposite time-variability pattern in trough width at the 95% continuum level ($w_{95}$) over the five epochs. Implications of these observational results will be discussed in Section 5.

### 3.3. J0136: A Case with Strong Evidence for BAL Acceleration

J0136 was considered the strongest candidate for acceleration in Grier et al. (2016) based on the analysis of the C IV BAL profiles over different epochs. But the Al III BAL was mentioned only in passing in their work due to its shallow depth. Through a careful examination of the absorption features of different ions in velocity space, we found that this BAL absorber consists of Si IV, C IV, Al III, and Mg II. However, we did not explore Si IV in this work as it lies at the CCD blue edge. The Mg II absorption was detected only in the first two epochs and completely disappeared in later epochs. Such a phenomenon, in which lower-ionization BAL species disappear faster than higher-ionization BAL species at the same velocity, has also been reported in other quasars in the literature (see Wang et al. 2015; Yi & Timlin 2021).

Through a detailed comparison between the C IV and Al III BALs over five epochs, we identified a number of interesting properties. (1) The centroid velocity of the Al III BAL increases monotonically with time, such that the velocity shifts relative to MJD 55444 are $-690 \pm 70$, $210 \pm 70$, and $230 \pm 70$ km s$^{-1}$ over the three time intervals (see cyan squares from the MJD versus $\Delta v_{\rm LOS}$ panel in Figure 4), respectively, consistent with those ($-760^{+101}_{-153}$, $185^{+52}_{-33}$, $170^{+68}_{-68}$) derived from the CCF analysis applied to the entire C IV BAL trough. (2) The Al III/Mg II BAL components completely disappeared while the C IV BAL component decreased by a factor of 2 in REW from the first to last epoch. (3) The C IV BEL decreased by a factor of $\sim$2 in REW while the Al III/Mg II BELs remained generally unchanged over the epochs. (4) The C IV BAL and BEL have a similar time-variability pattern characterized by an overall decrease of REW with time. (5) The Al III trough becomes wider after the first epoch, consistent with the broadening effect from acceleration (see Section 5.1.1), although we cannot rule out other possibilities. Unlike in J1344, the Al III BAL in J0136 completely disappeared while its Al III BEL strength remained generally unchanged over the epochs. Regarding the relation of the continuum and BEL variability, one has to consider the possibility of a time delay between them. However, a full investigation of the BEL variability requires higher-cadence spectroscopic observations on longer timescales, which is beyond the scope of this work.

J0136 shows kinematic acceleration signatures traced by both the C IV and Al III BAL troughs, in which the latter completely disappeared by MJD 59516 characteristic of a LoBAL $\rightarrow$ HiBAL transformation in tandem with the acceleration. Examining the MJD versus $f_{1700}$ panel, the continuum flux density at $\lambda_{\rm rest} = 1700$ Å brightened by a factor of $\sim$2 during the BAL transformation, a variability pattern that was also reported in another LoBAL quasar undergoing the same transformation (Yi et al. 2022). However, the variability relation between velocity shift and continuum flux is unclear for J0136, given both the same and opposite trends observed over different time intervals, such that the largest velocity shift occurred in the interval with no or small-amplitude continuum variability, while the largest-amplitude continuum variability was detected in the interval having only a small velocity shift along with the Mg II BAL disappearance. These results will be discussed in Section 5.

### 3.4. J1238: A Case with Tentative Evidence for BAL Acceleration

The spectra of J1238 show that the Mg II BAL profiles are very similar to each other and contain at least three BAL subflows in each epoch (see the left panel of Figure 5). Although each subflow may be composed of many Mg II doublets, we are unable to identify them due to saturation, self-blending, insufficient spectral resolution, and potential overlap with Fe II. The deepest two BAL subflows, at $\lambda_{\rm rest} \sim 2700$ and $\sim$2735 Å, vary in depth and velocity from epoch to epoch, while the shallowest BAL subflow at $\lambda_{\rm rest} \sim 2650$ Å appears

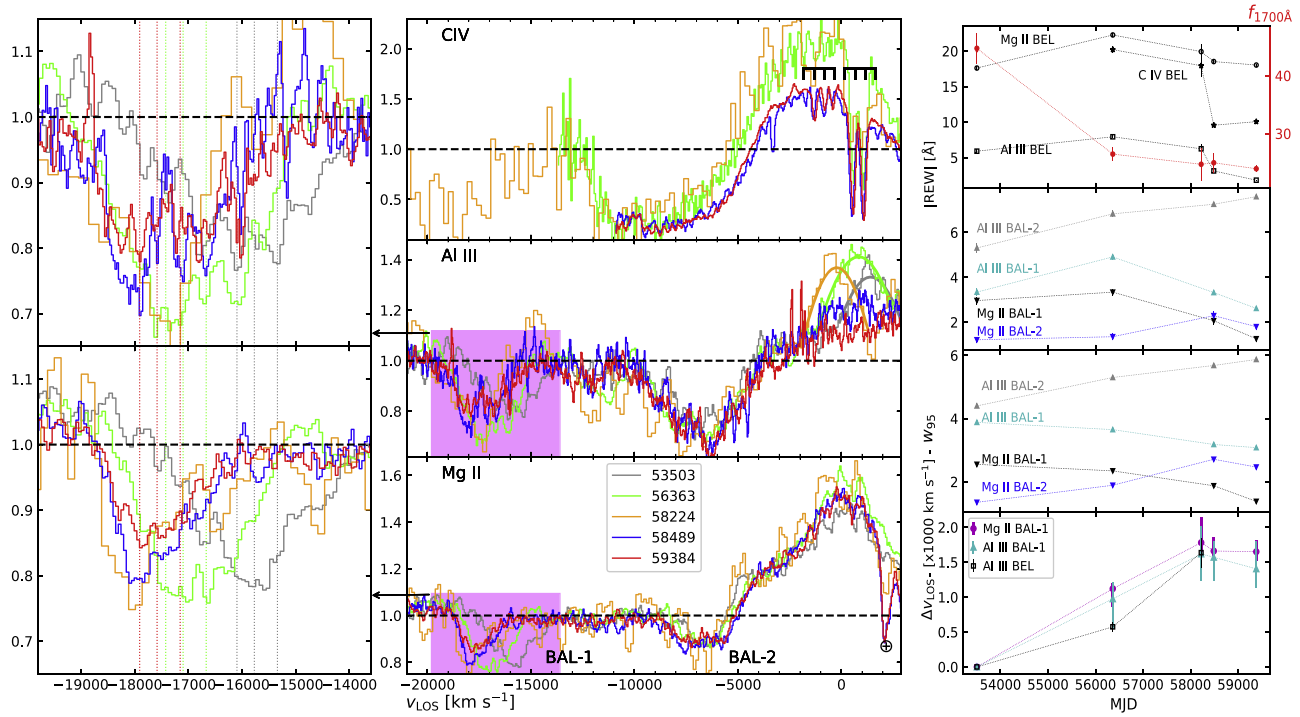


**Figure 3.** Left: zoom-in profiles of the BAL-1 in Al III and Mg II, in which a set of three blueward components of the Al III and Mg II doublets (gray/green/red vertical dotted lines) with two fixed velocity separations is identified in each of the three spectra with relatively high S/N, indicative of the same BAL-1 subflow persisting over the epochs. Middle: continuum-normalized spectra of the group-1 quasar J1344, in which two distinct BALs are labeled with BAL-1 and BAL-2. The comb-like symbols in the middle subpanel indicate radiative-acceleration, line-locking signatures of C IV. The Earth symbol in the bottom left subpanel indicates telluric absorption. The three bell-like profiles depict the one-Gaussian fits to the apparent Al III BEL peaks. Right: MJD vs. velocity shifts (relative to the first epoch), trough widths ($w_{95}$; trough width at the 95% continuum level), REWs (the Al III emission peak nearly disappeared at MJD 59384), and continuum flux at $\lambda_{rest} = 1700$ Å.

not to change in depth. In addition, the He I* $\lambda$10830 BAL profile is very similar to the Mg II BAL trough except for its depth (see Section 4.2).

The continuum flux density, however, increases monotonically with time over the four epochs as shown by the *V*-band magnitudes (see the black circles in the MJD versus Mag panel of Figure 5, in which the last two *V*-band magnitudes are converted from their ZTF-$g/r$ magnitudes; see Jester et al. 2005). Interestingly, the strength of the Mg II/He I* $\lambda$3889 BAL decreased/increased between MJD 54243 and 56035 while both increased between MJD 58198 and 59306, despite the increase in continuum flux over both intervals. Such complex BAL-variability behaviors are consistent with previous studies that disfavor the pure ionization-change scenario (McGraw et al. 2017; Yi et al. 2019).

In the analysis of BEL variability, one must keep in mind that the complex emission at 2750 Å $< \lambda_{rest} <$ 3000 Å appears to be dominated by Fe II rather than Mg II, given the generally unchanged Mg II BEL as opposed to large variability in the Fe II BEL at 2815 Å $< \lambda_{rest} <$ 2900 Å from MJD 54234 to 58198. Nevertheless, the Mg II BEL profile is asymmetric and exhibits a blueshift relative to systemic redshift; in addition, the Mg II BEL weakened dramatically from the first to last epoch, perhaps leading to the apparent increase of the Mg II BEL blueshift. The Mg II BAL and BEL show an overall opposite time-variability pattern, which will be discussed in Section 5 in conjunction with J0136 and J1344.

Compared to BAL-1 in J1344, which exhibits a large kinematic shift over the rest-frame 6.6 yr, the Mg II BAL in J1238 has much smaller kinematic shifts ($\Delta v_{LOS} = -257^{+60}_{-33}$, $+150^{+220}_{-330}$, $-210^{+67}_{-130}$ km s$^{-1}$) relative to the first epoch over the three time intervals after performing the CCF analysis as demonstrated above, perhaps indicative of milder acceleration/deceleration events. The evidence for BAL acceleration remains tentative due to the low spectral resolution at MJD 58198. Alternatively, using the deepest BAL subflow, we found that its characteristic velocity has also experienced a decrease → increase → decrease process. These results support both acceleration and deceleration events occurring at least for the deepest BAL subflow, if not for the entire BAL trough. Again, no clear relations have been found between velocity shift ($\Delta v_{LOS}$) and continuum flux, in agreement with J0136. This variability behavior will be discussed in Section 5.

### *3.5. J1259: A Case with Tentative Evidence for BAL Acceleration*

As reported in the discovery paper from Hall (2007b), the optical spectrum of J1259 is notably characterized by Balmer absorption features, a rare phenomenon observed in BAL quasars. Since a BAL seen in a singlet such as H9 is naturally expected to be narrower than that from a doublet such as C IV, we treat these Balmer absorption features in J1259 as "BALs" throughout this work. Note that these Balmer troughs have an overlap with the Mg II BAL in LOS velocity, and at least the H$\gamma$ trough at MJD 58216 is consistent with a bona fide BAL. From subsequent studies of this quasar (e.g., Shi et al. 2016; Yi et al. 2019), significant variations were detected for both the Balmer and Mg II BALs based on the analysis of the two SDSS spectra (MJD 53473 and 55983). Although Shi et al. (2016) proposed that BAL acceleration likely occurred in this quasar,

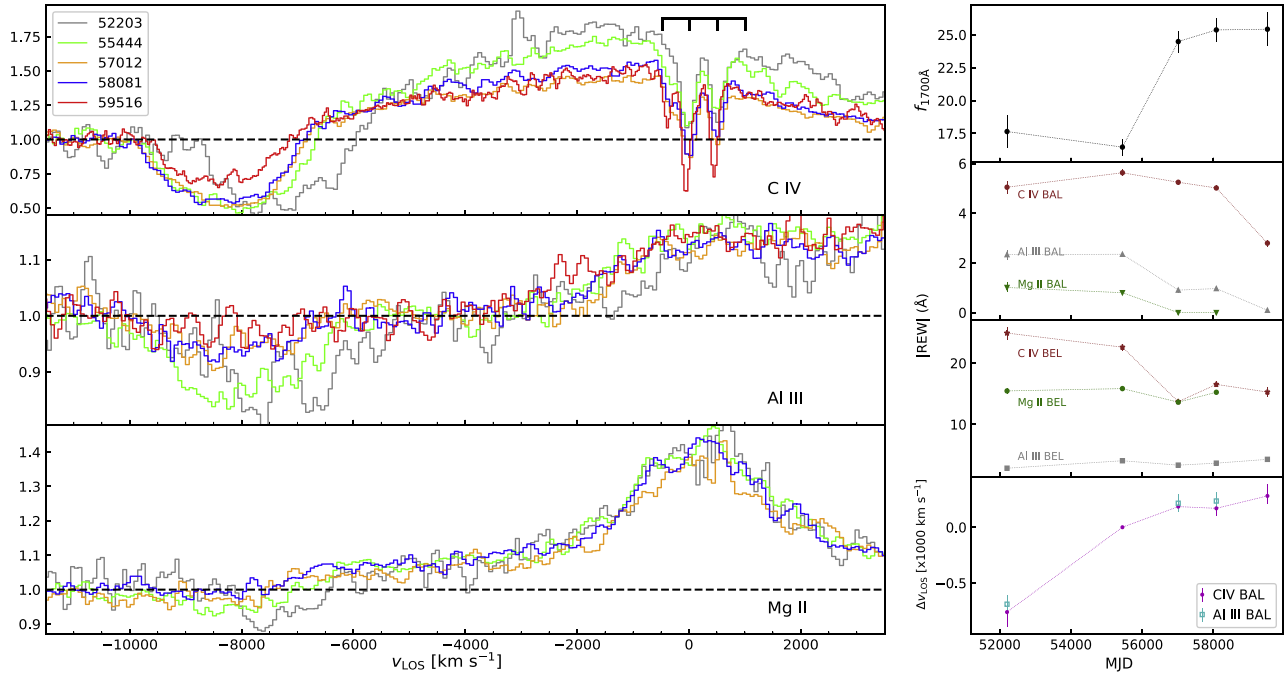


**Figure 4.** Left: continuum-normalized spectra of the group-1 quasar J0136 over five epochs. The comb-like symbol again indicates a line-locking feature in C IV. Right (bottom to top): MJD vs. velocity shifts of the C IV BAL relative to MJD 55444, REWs for the BALs and BELs, and continuum flux at $\lambda_{\rm rest} = 1700$ Å, which depict the time-variability behaviors of these quantities. The C IV BAL profiles are identical (CCF coefficient $> 0.9$) to that from MJD 55444 and the velocity shifts in each interval measured by the two different methods are consistent within measurement errors. The Mg II was caught on the disappearance as opposed to the persistence of C IV from the BAL flow.

evidence for acceleration remains lacking due to limited sampling epochs in their work. With the aid of four additional optical spectra obtained by HET/LRS-2, LJT/YFOSC, and LBT/MODS, we are now able to assess BAL acceleration in considerable detail by analyzing the similarities and differences among the six spectra from different epochs (over ∼9 rest-frame years) for this quasar.

To alleviate contamination from telluric absorption and blending with other ions (for details see Hall 2007b; Shi et al. 2016) during the analysis, we choose to examine the H9 and Hγ absorption features since they consist primarily of a single ion with relatively high spectral S/N. It is obvious from Figure 6 that the two BAL profiles varied most dramatically during the time interval from the first to second epoch, but changed only slightly over the later epochs. Therefore we adopt the second-epoch spectrum as the benchmark when applying the CCF analysis to this quasar. The CCF coefficient ($\rho = 0.74$) is lowest for the epoch pair between MJD 53473 and 55983, consistent with our visual observation that the Hγ BAL profile at the first epoch appears to be somewhat different from those at other epochs. In addition, we visually examine the absorption peaks across the two BAL troughs from different ions over the epochs, whose differences may trace the velocity shift when assuming that the same BAL subflow persists in each epoch.

The Hγ BAL spectral region has the highest S/N among these Balmer lines, so it is used as a benchmark to search for absorption peaks and velocity shifts over the epochs for this quasar. In Figure 6 the red vertical line indicates the peak absorption at the first epoch and is shown in the same column for easy comparison, while the positions of peak absorption are indicated by the blue vertical lines in the other five epochs. The Hγ absorption peak is consistent with that of the H9 BAL in each epoch. Therefore, using the deepest absorption feature as a characteristic velocity of the BAL absorber, we also found that the BAL velocity increases monotonically from MJD 53473 to 58601 and decreases slightly over the later two epochs, indicative of BAL acceleration and perhaps deceleration for this quasar. Quantitatively, the velocity shifts traced by the peak absorption of Hγ over the other five successive epochs are $657 \pm 70$, $795 \pm 70$, $1072 \pm 260$, $806 \pm 70$, and $855 \pm 70$ km s$^{-1}$ relative to the first epoch. The last four velocity shifts are therefore $138 \pm 70$, $415 \pm 260$, $149 \pm 70$, and $198 \pm 70$ relative to the second epoch, which are in agreement with those ($173^{+140}_{-70}$, $410^{+117}_{-117}$, $242^{+13}_{-69}$, $311^{+20}_{-69}$ km s$^{-1}$ relative to the trough at MJD 55983) derived from the CCF analyses to all but the first-epoch spectra having an overall identical Hγ BAL profile as tested by the maximum CCF coefficient ($\rho > 0.9$ versus $\rho = 0.74$). This result reinforces the argument for BAL acceleration. However, the above results provide only tentative evidence of BAL deceleration, due to a large uncertainty from the low-S/N, low-resolution spectrum at MJD 58601.

It is worth noting that the [O II] emission line in J1259, at first glance, appears to have experienced a sudden disappearance at MJD 58894 and a reappearance at MJD 59308 (see Figure 6). However, the integral field unit data at both MJD 58216 and 59308 reveal a similar one-sided, off-nuclear [O II] emission nebula with a projected size of ∼25 kpc (W. Yi et al. 2024, in preparation). Therefore, a long-slit spectroscopic observation that was targeting the quasar core could make the [O II] emission photocenter fall out of the slit with PA = 328°, leading to the apparent disappearance of [O II] from the long-slit, background-subtracted spectrum at MJD 58894. On the other hand, the [O III] emission exhibits a blueshifted, broad-wing feature in each epoch, suggesting that some of the BAL winds may be closely linked to the forbidden-line outflows. A dedicated study, especially via spatially resolved 3D spectroscopy, would be valuable to gain unique insights into the origin

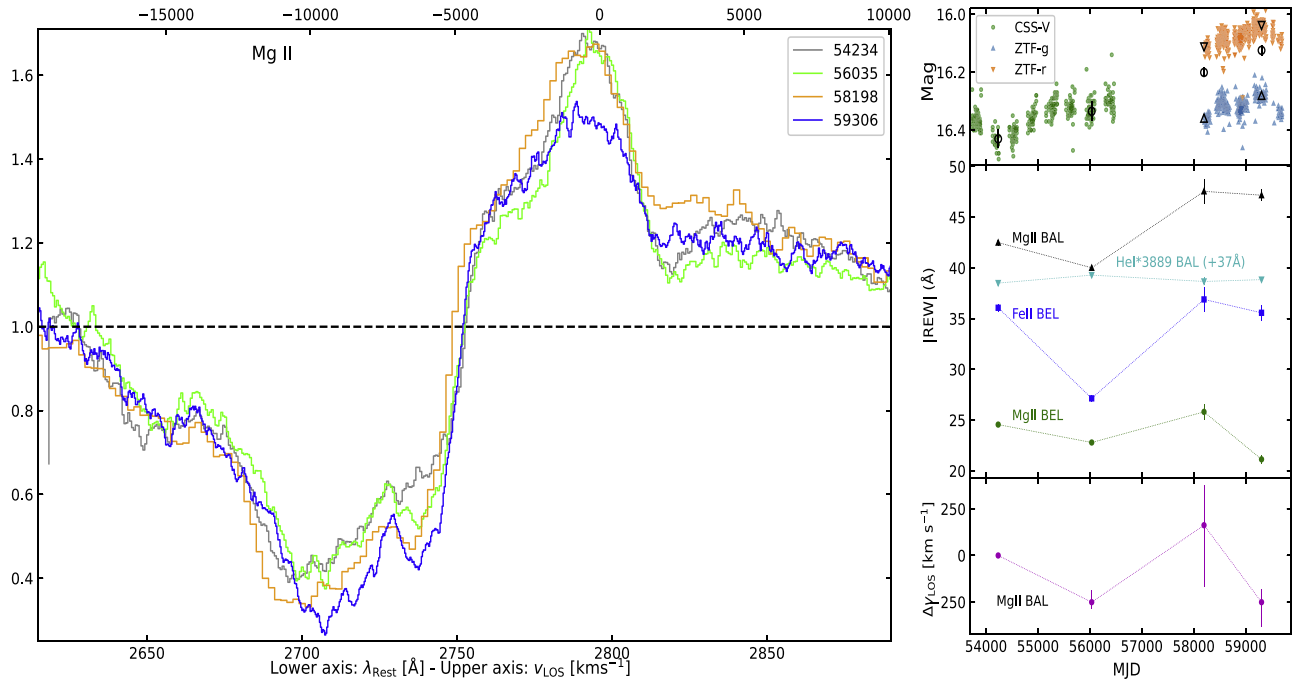


**Figure 5.** Left: continuum-normalized spectra of the group-2 quasar J1238 for the Mg II BAL/BEL over four epochs. Right (bottom to top): MJD vs. velocity shift of the Mg II BAL, REW for the BALs and BELs, and photometric magnitudes, which depict the time-variability patterns of these quantities. Unlike the Mg II BAL, which has at least three subflows, the He I* BAL is detected only at $v_{LOS} \sim 6000$ km s$^{-1}$ (see Section 4.2) and offset above by 37 Å for clarity. The positive/negative velocity shifts detected over the epochs may be linked to BAL acceleration/deceleration events for this quasar.

of the giant [O II] nebula; this effort is beyond the scope of this work. We briefly discuss the implications of these results in Section 5 after combining the other three quasars, particularly in the context of hot dust and weak radio emission.

### 3.6. An Overall View of BAL Acceleration

The two quasars from group 1 possess multiple BAL-acceleration signatures. J1344 is the most convincing example of BAL acceleration known to date, given that (1) the BAL profiles of interest are similar over the epochs except for differences in velocity shift; (2) the velocity shifts over each time interval measured by two different methods are approximately equal; (3) its largest BAL-velocity shift in Mg II (1780 km s$^{-1}$) is much higher than the median value (98 km s$^{-1}$) of positive velocity shifts + 3$\sigma$ uncertainties from Table 4 in Grier et al. (2016) (see Figure 7); and (4) most importantly, our data reveal the velocity shift in J1344 as a linear function of time interval over three well-separated, consecutive epochs, which is highly unlikely to be caused by BAL-profile variability and other random effects. J0136 (another quasar in group 1) has all but property (4) listed above, which can be considered a less robust but still convincing example of BAL acceleration.

In contrast, BAL-acceleration signatures of the two quasars from group 2 are less convincing than those from group 1, due to smaller BAL shifts and the lack of widely separated doublets such as Al III that can be well resolved by the intermediate-resolution spectroscopy. The Mg II doublet has a shorter wavelength separation than Al III and is often unidentifiable from a BAL trough due to saturation and blending with Fe II. However, the group-2 quasars still have negative BAL-velocity shifts at a significant level relative to the measurement uncertainties (–260 ± 70/–270 ± 70 km s$^{-1}$ for J1238/J1259); moreover, these negative shifts are almost 3 times higher than the median value (–102 km s$^{-1}$) of negative velocity shifts – 3$\sigma$ uncertainties from Grier et al. (2016), supportive of BAL deceleration. Note that the smaller the BAL-velocity shift between two epochs, the greater the chance that the shift could be due to velocity-dependent changes in trough depth caused by changes in ionization and/or transverse motions, and not bulk acceleration or deceleration. Table 2 provides an overall view of the spectral measurements.

## 4. Multiwavelength Information

### 4.1. Properties of the Spectral Energy Distribution

This section explores the properties of the spectral energy distribution (SED) for each of the four quasars, focusing particular attention on variability of the rest-frame UV reddening between two different epochs. J0136 and J1344 are BAL-acceleration candidates without significant radio detections from the Faint Images of the Radio Sky at Twenty-Centimeters (FIRST), while J1238 and J1259 exhibit signatures of both BAL acceleration and deceleration, along with weak radio emission and a much redder color as indicated by the W3/SDSS-$i$ ratio.

Figure 8 displays the SEDs of the four quasars, whose photometric data are retrieved from Galaxy Evolution Explorer (GALEX), SDSS, Two Micron All Sky Survey (2MASS), Wide-field Infrared Survey Explorer (WISE), and FIRST sky surveys (see Lyke et al. 2020 and references therein). To highlight variability in the rest-frame UV continuum, we display the early/late epoch spectra in red/blue for each quasar. In addition, the near-IR spectra obtained by P200/TripleSpec for J0136 and J1238 are flux-corrected by the photometric data from 2MASS and included in their SEDs for comparison. All the four SEDs have a peak at $\lambda_{rest} \sim 10$ $\mu$m; in

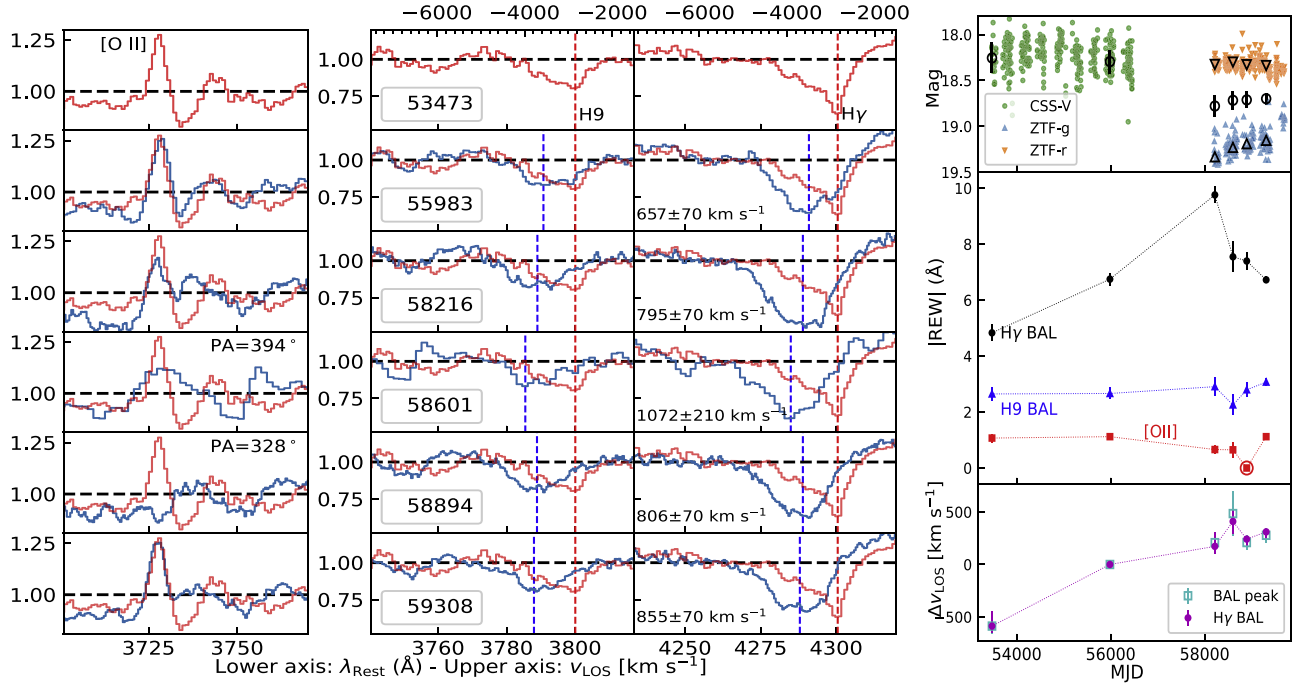


**Figure 6.** Left: continuum-normalized spectra of the group-2 quasar J1259 over six epochs. The vertical red/blue dashed lines refer to the peak absorption at the first/other epochs, from which one can directly see how the velocity shift varies with time using the first epoch as a benchmark (the first spectrum is superimposed on all successive epochs and the positions of the red and blue dashed lines in H9 are fixed by those of Hγ). Apparently, H9 remains generally unchanged in REW while the Hγ BAL appears to vary from epoch to epoch. Right (bottom to top): MJD vs. velocity shift of the Hγ BAL relative to MJD 55983, REWs of different ions, and photometric magnitudes. The apparent disappearance in [O II] emission at MJD 58894 (highlighted by the red circle) is due to a rotation (marked by position angle (PA) from the left panels) between the two long-slit spectroscopic observations targeting the quasar core with a one-sided, off-nuclear [O II] emission nebula (W. Yi et al. 2024, in preparation).

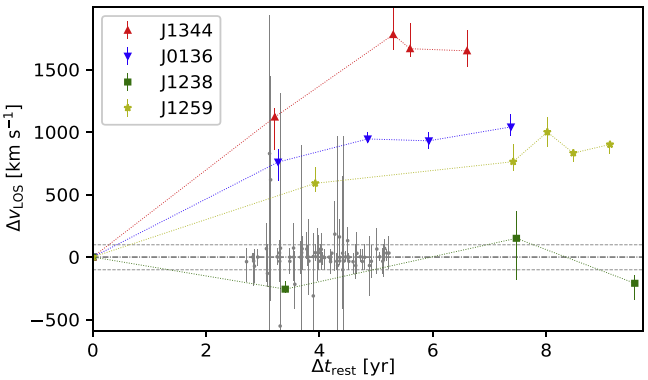


**Figure 7.** Comparison between the LoBAL (color) and HiBAL (gray; from Table 4 of Grier et al. 2016) samples. The two horizontal dotted lines are the upper limits of BAL acceleration/deceleration in Grier et al. (2016) derived from the median values of velocity shifts + $3\sigma$ positive/negative uncertainties. J1344, J0136, and J1259 all show a similar trend, such that they have a steep rise followed by a plateau-like time evolution in BAL-velocity shift.

particular, the group-2 quasars have a steeper rise of the SED shape than the group-1 quasars at $1\ \mu\mathrm{m} < \lambda_{\mathrm{rest}} < 3\ \mu\mathrm{m}$.

J0136 is the only one among the four quasars undergoing a LoBAL → HiBAL transformation and becoming brighter/bluer in the rest-frame UV band at later epochs. Interestingly, such a time-variability trend is also seen in six LoBAL quasars that were caught in a LoBAL → HiBAL transformation (Yi & Timlin 2021); in particular, the C IV, Al III, and Mg II BAL-variability trends in J0136 resemble closely another LoBAL quasar (J0827) that was captured in shedding its dust cocoon, despite the emergence of a new C IV BAL in J0827 (see Figure 4 in Yi et al. 2022). Given the persistence of the BAL in J0136 and the LoBAL → HiBAL → non-BAL evolutionary path proposed in Yi & Timlin (2021), we argue that the SED of J0136 will become increasingly bluer/brighter, and ultimately, like the vast majority of non-BAL blue quasars, will peak at the rest-frame UV band as time passes. In contrast, J1344 is still in a LoBAL state and becomes conspicuously dimmer (by a factor of ∼2) in the UV continuum over the later epochs, although it has an even larger BAL-acceleration magnitude than J0136 (1.14 versus 0.74 cm s$^{-2}$; see Table 2). These results are valuable for advancing our understanding of the nature of BALs, which will be discussed in Section 5 in conjunction with the multiwavelength data at hand.

### 4.2. Near-IR Spectroscopy for J1238 and J0136

We have performed near-IR spectroscopic observations using the P200/TripleSpec for J1238 and J0136. The near-IR spectrum of J0136 at MJD 59503 exhibits strong Fe II and weak H$\beta$ emission (see left panels of Figure 9). Following Yi et al. (2022), we use a model with two Gaussians and one Fe II component to fit the H$\alpha$ and H$\beta$ lines. Our spectral fit reveals that the H$\alpha$/H$\beta$ emission can be well fitted by two/one Gaussians, when their FWHMs are tied to each other and the H$\alpha$/H$\beta$ flux ratio is constrained within a range between 2.9 and 3.5 for one set of the Gaussians during the fit. The H$\beta$ FWHM of the broad-emission component is derived to be $2750 \pm 120$ km s$^{-1}$; in addition, the H$\alpha$ FWHM measured from a combination of the two broad Gaussians is $3200 \pm 50$ km s$^{-1}$, which is still narrower than that measured from the broad Mg II emission ($4650 \pm 19$ km s$^{-1}$; see Table 3 for individual components) at MJD 55444. This difference is expected in the context of stratified structures of the broad-line

**Table 2**
Measurements of the Rest Equivalent Widths, Trough Widths, Trough-velocity Shifts, and Acceleration Magnitudes

| Name | MJD | REW (Å) | REW (Å) | REW \| $w_{95}$ (Å \| km s$^{-1}$) | $\Delta v$ \| $a$ (km s$^{-1}$ \| cm s$^{-2}$) | $\Delta v$ \| $a$ (km s$^{-1}$ \| cm s$^{-2}$) |
|---|---|---|---|---|---|---|
| J1344 | | Mg II BAL-1 | Al III BAL-1 | Mg II BAL-2 | Mg II BAL-1 | Al III BAL-1 |
| | 53503■ | $2.96 \pm 0.17$ | $3.34 \pm 0.18$ | $1.2 \pm 0.12$ \| 1350 | ⋯ | ⋯ |
| | 56363 | $3.33 \pm 0.15$ | $4.9 \pm 0.13$ | $1.34 \pm 0.14$ \| 1890 | $1120^{+70}_{-260}$ \| $1.10^{+0.08}_{-0.26}$ | $980^{+230}_{-430}$ \| $0.97^{+0.22}_{-0.42}$ |
| | 58224 | $3.1 \pm 0.61$ | $3.76 \pm 0.60$ | $2.07 \pm 0.52$ \| ⋯ | $1780^{+360}_{-120}$ \| $1.06^{+0.22}_{-0.08}$ | $1620^{+390}_{-390}$ \| $0.97^{+0.23}_{-0.23}$ |
| | 58489 | $2.05 \pm 0.17$ | $7.21 \pm 0.27$ | $2.29 \pm 0.21$ \| 2712 | $1670^{+200}_{-65}$ \| $0.95^{+0.10}_{-0.03}$ | $1570^{+230}_{-330}$ \| $0.89^{+0.13}_{-0.18}$ |
| | 59384 | $1.27 \pm 0.11$ | $7.60 \pm 0.06$ | $1.80 \pm 0.13$ \| 2466 | $1650^{+160}_{-130}$ \| $0.79^{+0.08}_{-0.06}$ | $1410^{+400}_{-260}$ \| $0.68^{+0.18}_{-0.13}$ |
| J0136 | | Mg II BAL | Al III BAL | C IV BAL | C IV BAL | |
| | 52203 | $1.01 \pm 0.16$ | $2.33 \pm 0.20$ | $5.05 \pm 0.25$ \| 2560 | $760^{+101}_{-153}$ \| $0.74^{+0.09}_{-0.14}$ | ⋯ |
| | 55444■ | $0.84 \pm 0.10$ | $2.35 \pm 0.10$ | $5.63 \pm 0.13$ \| 2887 | ⋯ | ⋯ |
| | 57012 | ⋯ | $0.9 \pm 0.09$ | $5.25 \pm 0.08$ \| 2886 | $185^{+52}_{-33}$ \| $0.37^{+0.10}_{-0.07}$ | ⋯ |
| | 58081 | ⋯ | $0.97 \pm 0.09$ | $5.02 \pm 0.09$ \| 2684 | $170^{+68}_{-68}$ \| $0.20^{+0.07}_{-0.07}$ | ⋯ |
| | 59516 | ⋯ | ⋯ | $2.79 \pm 0.12$ \| 2258 | $281^{+105}_{-70}$ \| $0.22^{+0.08}_{-0.05}$ | ⋯ |
| J1238 | | Mg II BAL | He I* $\lambda$3889 | He I* $\lambda$10830 | Mg II BAL | Mg II BAL |
| | 54234■ | $42.50 \pm 0.27$ | $1.51 \pm 0.15$ | ⋯ | ⋯ | ⋯ |
| | 56035 | $40.01 \pm 0.22$ | $2.29 \pm 0.14$ | ⋯ | $-257^{+60}_{-33}$ \| $-0.24^{+0.06}_{-0.03}$ | ⋯ |
| | 58198 | $47.55 \pm 1.20$ | $1.67 \pm 0.37$ | $88.83 \pm 3.07$ \| 12350 | $150^{+220}_{-330}$ \| $0.06^{+0.10}_{-0.13}$ | ⋯ |
| | 59306 | $47.17 \pm 0.58$ | $1.85 \pm 0.17$ | ⋯ | $-210^{+67}_{-130}$ \| $-0.07^{+0.06}_{-0.04}$ | $a_{34} = -0.55^{+0.07}_{-0.09}$ |
| J1259 | | H9 BAL | | H$\gamma$ BAL | H$\gamma$ BAL | H$\gamma$ BAL |
| | 53473 | $2.65 \pm 0.24$ | ⋯ | $4.83 \pm 0.29$ \| 1707 | $590^{+130}_{-70}$ \| $0.48^{+0.12}_{-0.06}$ | ⋯ |
| | 55983■ | $2.66 \pm 0.20$ | ⋯ | $6.75 \pm 0.22$ \| 1910 | ⋯ | ⋯ |
| | 58216 | $2.91 \pm 0.33$ | ⋯ | $9.76 \pm 0.30$ \| 2347 | $173^{+140}_{-70}$ \| $0.16^{+0.12}_{-0.06}$ | ⋯ |
| | 58601 | $2.26 \pm 0.42$ | ⋯ | $7.55 \pm 0.55$ \| 2143 | $410^{+117}_{-117}$ \| $0.32^{+0.09}_{-0.09}$ | ⋯ |
| | 58894 | $2.79 \pm 0.25$ | ⋯ | $7.40 \pm 0.32$ \| 2332 | $242^{+13}_{-69}$ \| $0.17^{+0.01}_{-0.05}$ | $a_{45} = -1.17^{+0.13}_{-0.13}$ |
| | 59308 | $3.07 \pm 0.13$ | ⋯ | $6.72 \pm 0.12$ \| 2161 | $311^{+20}_{-69}$ \| $0.19^{+0.01}_{-0.04}$ | ⋯ |

**Note.** (1) The square represents the benchmark spectrum used for the CCF analysis for each quasar. (2) $w_{95}$ is the trough width at the 95% continuum level. (3) $a_{34}$ and $a_{45}$ are the deceleration rates derived from the third/fourth and fourth/fifth epoch pairs, respectively.

region (BLR) for the Mg II and H$\alpha$ emission, especially in the scenario where BAL winds are shaping the BEL profile of Mg II (see an example from Yi et al. 2022). Indeed, our spectral fit to the Mg II BEL reveals a blueshifted, narrow Gaussian that well characterizes the blueshifted-wing emission in Mg II (also see Figure 4 for a similar blueshifted feature over the other epochs), suggesting the presence of the Mg II emission-line outflows and hence making it less robust than H$\beta$ in the study of BLR physics. We caution that the H$\alpha$ and H$\beta$ FWHMs may be underestimated due to the CCD edge effect.

The near-IR spectrum of J1238 reveals a dramatic He I* $\lambda$10830 absorption feature aligning exactly with the Mg II BAL trough in velocity space, whose kinematics is very similar to the Mg II BAL trough characterized by three major BAL subflows (see right panels of Figure 9). However, the multiepoch optical spectra indicate that the corresponding He I* $\lambda$3889 absorption is detected only for the BAL subflow at $v_{\rm LOS} \sim -6000$ km s$^{-1}$ and remains generally unchanged over the epochs, characteristic of an absorber that has a partial covering factor in He I* and is more saturated than other subflows across the entire He I* BAL trough. Nevertheless, both the He I* and Mg II troughs must be saturated to some extent, because theoretically the optical-depth ratio between He I* $\lambda$10830 and $\lambda$3889 for optically thin gas is 23.3 (Leighly et al. 2011), whereas this ratio in the spectra of J1238 is only ∼6.5 from the velocity range where the $\lambda$3889 feature is seen, according to the apparent optical depth $\tau_a(v) = \ln[I_0(v)/I_{\rm obs}(v)]$, where $I_0(v)$ and $I_{\rm obs}(v)$ are the intrinsic and observed fluxes at velocity $v$, respectively.

## 5. Discussion

### 5.1. Implications from Joint Analyses

The four quasars, especially those from group 1, are promising candidates for BAL acceleration based on our analyses, although other possibilities may contribute secondarily to the BAL-velocity shift. They will be treated as actual BAL-acceleration quasars throughout the following sections to explore some of the key questions of quasar feedback, such as the driving force of BAL acceleration, the process of BAL winds coupling to the ambient medium, and potentially observable imprints during the BAL-acceleration phase. Acceleration is the simplest and most straightforward interpretation for a monolithic velocity shift of a BAL seen from multiepoch spectra, i.e., one would expect to see increasing/decreasing portions of the BAL blue/red wings in cases of acceleration or decreasing/increasing portions of the BAL blue/red wings in cases of deceleration. Below we explore the implications of BAL acceleration and then deceleration in conjunction with the multiwavelength data at hand.

#### 5.1.1. The Driving Mechanisms of BAL Acceleration

One of the long-standing questions about BAL winds is the driving mechanism. Theoretically, BAL winds with LOS velocities above 5000 km s$^{-1}$ are thought to be driven by UV radiation pressure on ionized gas within $R \lesssim 1$ pc from the quasar center, when noticing that the typical SEDs of normal quasars peak at the UV band, despite some debates about the

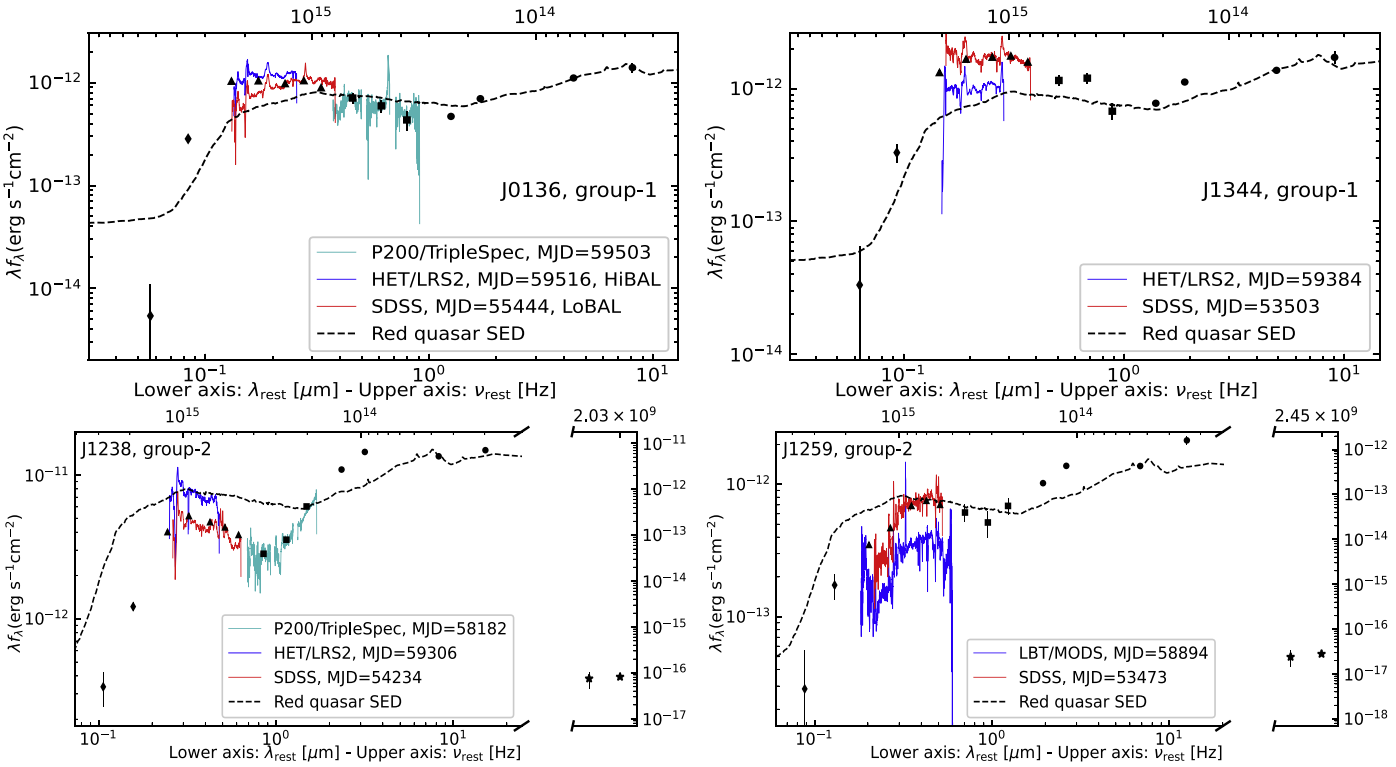


**Figure 8.** SEDs of the four quasars, which incorporate data from GALEX (diamonds), SDSS (triangles), 2MASS (squares), WISE (circles), and VLASS and FIRST (stars). The early/late epoch spectra are shown in red/blue for each quasar, complemented with a near-IR (cyan) spectrum if it exists. J0136 and J1344 (group 1) have BAL-acceleration signatures and are radio-quiet; in addition, J0136 is undergoing a LoBAL → HiBAL transformation along with an increase in brightness over the epochs, while J1344 remains in a LoBAL state along with a decrease in brightness. J1238 and J1259 (group 2) exhibit BAL-acceleration/deceleration signatures and weak radio emission, with $f_{3\rm GHz}/f_{1.4\rm GHz} = 2.5/5.84$ mJy and $0.8/2.0$ mJy for the former and latter, respectively. The GALEX photometry for J1259 should be treated with caution given its large flag values. The median SED of red quasars from Calistro Rivera et al. (2021) is scaled to the W3 band.

role of shielding gas (e.g., Murray et al. 1995; Proga et al. 2000; Hamann et al. 2019). This scenario is supported by observations and appears particularly true for LoBAL quasars, in that they are more likely X-ray-weak and tend to possess softer ionizing SEDs than normal quasars (e.g., Gallagher et al. 2006; Trump et al. 2006; Hamann et al. 2019).

In addition to UV radiation-driven winds on small scales, IR radiation pressure on dust, e.g., via IR photon trapping and multiple scattering processes, may provide an additional force to accelerate ionized outflows on large scales, particularly when they are mildly optically thick to IR radiation and effectively coupled to dust (e.g., Costa et al. 2018). Other driving mechanisms, such as magnetic fields or cosmic rays, may also be at work or coexist with the above two forces for accelerating BAL winds, but we are unable to assess these possibilities using the current data. Therefore, throughout the discussion we will ignore them and focus only on the UV/IR radiation-driven scenarios.

Unlike high-velocity, UV radiation-driven disk winds that are thought to be launched at $R \sim 0.01$ pc, IR radiation-driven outflows must exist in large-scale regions ($R \gtrsim 1$ pc) where dust can survive; hence, relatively low-velocity ($<$3000 km s$^{-1}$) outflows and small acceleration magnitudes may be expected if driven solely by IR radiation (e.g., Faucher-Giguère & Quataert 2012; Roth et al. 2012; Costa et al. 2018). Recently, He et al. (2022) found from a small sample that BAL velocities appear to increase with galactocentric distances, from which they interpreted that UV radiation pressure on dust is the driving force of BAL acceleration, despite the lack of investigations in kinematic shift as adopted routinely in previous studies for acceleration, and the unknown coupling efficiency between dust and gas in that work. Nevertheless, IR radiation pressure on dust can exert an additional force to a high-velocity BAL wind that is located at relatively large radii (e.g., $R > 1$ pc), leading to mild BAL acceleration as seen in group-2 quasars.

Although the IR radiation-driven scenario offers a possible explanation for the rarity of BAL acceleration as reported in Grier et al. (2016), it appears difficult to explain the large BAL-acceleration magnitudes seen in the group-1 quasars. While the large BAL acceleration from group 1 is likely driven by UV radiation pressure at relatively small radii (e.g., $R < 1$ pc), the dust responsible for UV extinction/suppression may not necessarily be related to the presumably traditional torus with $R < 10$ pc; instead, dust could reside in a broad range of regions (e.g., Hamann et al. 2017; Temple et al. 2019; Calistro Rivera et al. 2021). Thus, whether a BAL wind, which is launched from its accretion disk, has reached a circumnuclear region or beyond is crucial for the discussion. A combined analysis of the BAL, BEL, and continuum time-variability behaviors can provide valuable diagnostics, which are discussed below.

One of the most striking differences between the two group-1 quasars is the opposite time-variability pattern in UV continuum flux, such that J0136/J1344 become brighter/fainter in later epochs. If UV radiation is the dominant driver for the observed BAL acceleration, one may expect to see a strong correlation between the continuum flux and BAL-velocity shift. Indeed, the largest velocity shift (acceleration) occurs in the time interval along with a decrease in UV

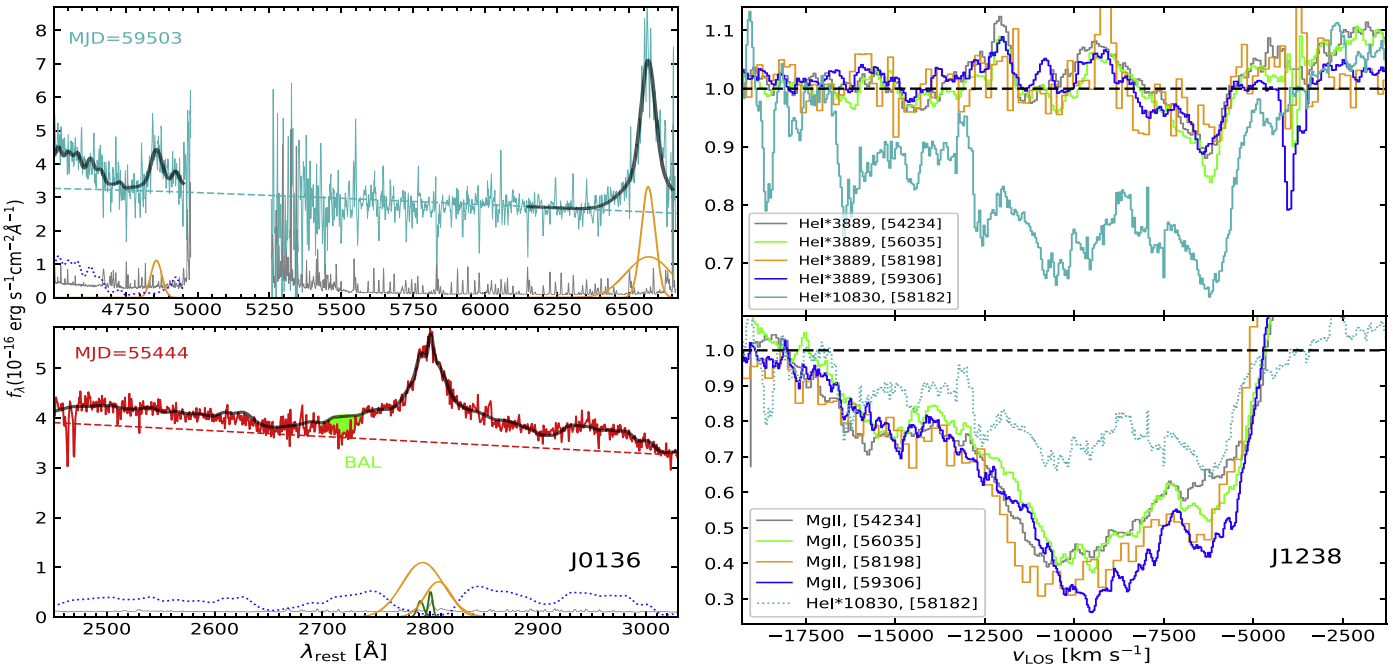


**Figure 9.** Left panels: the spectral fits (thick gray) to the Mg II (bottom panel), H$\beta$, and H$\alpha$ (top panel) emission for J0136, which include the Fe II (blue dotted), the broad Gaussians (orange), the narrow Gaussians (green), and the continuum fits (dashed). The BAL feature (green) was masked during the fit. The thin gray lines indicate spectral errors. The fits indicate that FWHM(Mg II) is ∼4650 km s$^{-1}$ in broad emission as opposed to FWHM(H$\beta$) ∼2750 km s$^{-1}$, and that blueshifted emission/absorption features exist in Mg II but not in H$\beta$, suggestive of the former being more affected by outflows. Right panels: the He I$^*$ $\lambda$10830 and $\lambda$3889 BAL profiles for J1238. For comparison, a subpanel of the Mg II BAL profile is added over the four epochs, above which the He I$^*$ $\lambda$10830 BAL is displayed. Unlike the He I$^*$ $\lambda$10830 and Mg II BALs, which have three major subflows, only one He I$^*$ $\lambda$3889 BAL feature was detected at $v_{\rm LOS} \sim -6000$ km s$^{-1}$, whose strength remains generally unchanged over the epochs.

**Table 3**
Spectral Fitting Results of the BELs for J0136

| | $\lambda_c$ FWHM \| (Å) \| (km s$^{-1}$) | | | |
|---|---|---|---|---|
| | BG-1 | BG-2 | NG-1 | NG-2 |
| Mg II | 2808 \| 3102 | 2793 \| 4806 | 2791 \| 750 | 2800 \| 501 |
| H$\beta$ | 4860 \| 2750 | ⋯ | ⋯ | ⋯ |
| H$\alpha$ | 6564 \| 2680 | 6570 \| 8346 | ⋯ | ⋯ |

**Note.** BG and NG refer to the broad and narrow Gaussians decomposed from the spectral fitting; $\lambda_c$ refers to the center of the rest-frame wavelength of a specific Gaussian.

continuum for both quasars (see Figures 3 and 4); thus, the two quantities may always exhibit an opposite time-variability pattern during an acceleration phase, or the variability in UV continuum may be only loosely coupled to the variability in the incident ionizing continuum seen by the BAL gas. In contrast, the two quantities appear to display an opposite variability behavior for J1259 in the interval from MJD 55983 to 58216 but a similar variability behavior in the interval from MJD 58216 to 58601. On the other hand, a much redder color in group 2 than in group 1 again supports a different acceleration mechanism, such as radiation pressure on dust from a large-scale region.

For the group-2 quasar J1259, Shi et al. (2016) inferred from the two SDSS spectra that a BAL absorber is likely located at a distance of $R \sim 1$ pc, on the basis of transverse motion as the cause of its BAL variability. This is also another reason for our caution in identifying any BAL acceleration based on only one spectroscopic pair. Suppose the same BAL absorber is persistent after the second epoch; one can see from the MJD versus Mag panel of Figure 6 that the ZTF-$g$ band monotonically brightens while the ZTF-$r$ band remains generally unchanged over the last four spectroscopic epochs. This result, at first glance, appears to be caused by the weakening H$\gamma$ trough after MJD 58216; however, it is difficult to explain the lack of significant variability in H9 (Figure 6). We suspect that it may signal a substantial decrease in dust or a change in dust distribution/composition along our LOS, because it is possible that the kinematic signatures of BAL acceleration/deceleration in J1259 trace the coupling process between dust and gas, i.e., radiation pressure on dust as a driver for launching outflows and interacting with the outer ISM. For the other group-2 quasar, J1238, the ZTF-$g/r$ bands show a similar light curve characterized by an increasing brightness over the last two spectroscopic epochs.

Interestingly, J1238 and Mrk 231 have many common features, such as the spectral shape, strong LoBAL (Mg II) and weak HiBAL (He I$^*$) troughs, strong Fe II and weak [O III] emission, potentially inner decelerated winds and outer accelerated outflows (the decreased portion of the BAL subflow at $-12{,}500$ km s$^{-1}$ $< v_{\rm LOS} < -10{,}000$ km s$^{-1}$ is comparable to the increased portion of the BAL subflow at $-7000$ km s$^{-1}$ $< v_{\rm LOS} < -5000$ km s$^{-1}$ from MJD 54234 to 56035; see Figure 9), and moderately weak radio emission. Therefore, like Mrk 231 having BAL distances at $R \sim 2$–100 pc, the BAL distance in J1238 may also cover a wide range (see Leighly et al. 2014; Veilleux et al. 2016). If this speculation is true, the mild acceleration seen in J1238 is also likely, at least partly, due to IR radiation pressure on dust, although we cannot exclude the possibility that UV radiation on ionized gas is the dominant driver for the initial BAL acceleration in both

quasars, particularly in cases where the dust and gas are not efficiently coupled.

For the group-1 quasar J1344, an intriguing result is the progressively broadening BAL-2 as opposed to the narrowing BAL-1, such that the width increment of BAL-2 is almost equal to the width decrement of BAL-1 from MJD 53503 to 59384 in both Al III and Mg II (see the MJD versus $w_{95}$ panel in Figure 3), possibly indicative of a new BAL-acceleration event characterized by a high-velocity inner wind (BAL-1 subflow) overtaking a low-velocity outer wind. This scenario is supported by the disappearance of both the Al III BAL (at $v_{\rm LOS} \sim -11{,}000\,{\rm km\,s^{-1}}$) and the Al III BEL peak, as well as the rapid drop of the C IV BEL strength after MJD 58224, an epoch when BAL-1 started to level off or perhaps decelerate. For the other group-1 quasar, J0136, the disappearance of LoBAL ions that are associated with a decrease in dust, could be the main cause of the brightening UV continuum; hence, its largest BAL acceleration magnitude, detected between MJD 52203 and 55444, could be dominated by UV radiation pressure on dusty gas. This interpretation is further supported by a decline in the acceleration magnitude after MJD 55444 (see Figure 4), an epoch when LoBALs and dust started to disappear along our LOS. It is worth noting that the time-resolved evidence for large-magnitude BAL acceleration along with line-locking, associated absorption lines (AALs; see Weymann et al. 1991 and references therein) seen in group-1 quasars, offers a plausible interpretation to link nuclear BAL winds and galactic AAL outflows, despite the huge difference in distance (<1 pc versus >1000 pc). As a comparison, spatially resolved evidence for small-magnitude acceleration/deceleration traced by the positive/negative correlations between [O III] emission-line width and velocity has been reported in the literature (e.g., FWHM increasing due to turbulence from acceleration or deceleration; see Figure 5 in Nesvadba et al. 2006). Therefore, spatially resolved spectroscopy of the BAL-acceleration quasars in the future may provide unique and valuable information to bridge the huge gap in distance.

A joint analysis of variability in both absorption and emission may offer additional diagnostics to further advance our understanding of BAL acceleration. It is clear that the BALs and BELs vary dramatically in J1344, while the Mg II/Al III BELs in J0136 remain generally unchanged as opposed to the complete disappearance of the Mg II/Al III BALs. In particular, the Al III BEL peak in J1344 exhibited a velocity shift comparable to that of the Al III BAL-1 in the interval from MJD 53503 to 58224, despite the different acceleration magnitudes measured in between. Such a difference can be explained by the complex structures and inner physics of the BEL outflows. Moreover, the Al III BEL in J1344 became progressively weaker after MJD 56363 (its peak nearly disappeared at MJD 59384; see Figure 3), which is again supportive of UV radiation pressure as a common driving force to accelerate both the BAL-1 and Al III BEL outflows. Given the brightening/dimming UV continuum detected in J0136/J1344, we argue that the absorption/emission-line variability behaviors, such as the monolithic BAL shifts and large REW drops of the C IV BEL, are loosely linked to UV continuum variability.

In addition, the BALs/BELs signal the LOS/bulk effects, respectively, which may also contribute to the differences in variability behaviors between J0136 and J1344. However, it remains difficult to explain (1) the opposite time-variability pattern in REW between BAL-1 and BAL-2 for J1344, and (2) the rapidly disappeared Al III BEL as opposed to the generally unchanged Mg II BEL for J1344 after MJD 58224. The second phenomenon may be linked to the third Al III BAL at $v_{\rm LOS} \sim -11{,}000\,{\rm km\,s^{-1}}$, whose variability behavior cannot be assessed in detail given its presence only at MJD 56363. Interestingly, both quasars show a common variability pattern in which the C IV BEL strength decreased by a factor of ∼2 near the point where the BAL velocity starts to level off, again supporting a connection between the BAL and BEL outflows; furthermore, both quasars exhibit slightly blueshifted, line-locking C IV signatures, indicative of quasar radiation-driven outflows coupled to the large-scale ISM.

It is worth noting again that the smaller the BAL-velocity shift between two epochs, the greater the chance that the shift could be due to velocity-dependent variability caused by ionization changes and/or transverse motions. Therefore, it is possible that another agent comes into play at some point in terms of curtailing acceleration, particularly when noticing the plateau-like trend among the three BAL-acceleration candidates (J0136, J1344, J1259) in later epochs (see Figure 7).

#### 5.1.2. BAL Deceleration as an Origin of Weak Radio Emission and Large-scale AALs

The presence of radio emission in BAL quasars remains unknown since BAL winds are thought to be launched from a viewing angle closer to the equatorial plane of the accretion disk than the jet (e.g., Becker et al. 2000; Yi et al. 2019; Nair & Vivek 2022). However, both theoretical and observational studies of the wind–ISM interactions predict the production of weak radio emission (e.g., Faucher-Giguère & Quataert 2012; Zakamska & Greene 2014), which was indeed detected in the group-2 quasars (J1238 with a flux density of 2.5/5.84 mJy and J1259 with a flux density of 0.8/2.0 mJy at 3.0/1.4 GHz, respectively). Interestingly, the two radio-band observations yield a spectral index of $\alpha \sim -1.1$ for both quasars, reinforcing the argument for the wind–ISM interaction as an origin of weak radio emission (Panessa et al. 2019). Moreover, all but J1344 were also detected by RACS at ∼800 MHz (∼8.3/2.2/1.7 mJy for J1238/J1259/J0136, respectively, while out of the survey range for J1344; McConnell et al. 2020), consistent with a higher radio detection rate at a lower frequency in the LoBAL population (Morabito et al. 2019). Given that the LoBAL quasar Mrk 231 also has moderately weak radio emission along with evidence for BAL deceleration/acceleration and radio flares, we propose an underlying link between the two phenomena, which can be tested with follow-up observations in the future.

As a comparison, Shi et al. (2016) speculated that the Balmer absorber in J1259 experienced deceleration due to the collision with the surrounding medium, based on an analysis of the two SDSS spectra. In combination with the observational results from six optical spectra and multiwavelength data, we did find additional evidence in support of wind deceleration for J1259. Furthermore, such deceleration events can explain the high incidence of weak radio emission among red quasars that appears to peak around the radio-quiet and radio-loud threshold (Klindt et al. 2019), given an anomalously high fraction of BALs seen in red quasars (e.g., Urrutia et al. 2009; Fynbo et al. 2013; Hamann et al. 2017) and a high radio detection rate found in the BAL population (e.g., Morabito et al. 2019; Yi et al. 2019).

Like the group-1 quasars, three X-ray-bright BAL quasars from Joshi et al. (2014, 2019) also possess AALs and kinematic signatures of BAL deceleration. The lack of significant velocity shifts in AALs, as opposed to large BAL-velocity shifts found in both this work and Joshi et al. (2014, 2019), suggests that large-magnitude, identifiable acceleration events mostly occur in BALs rather than AALs, consistent with the latter being located in a large-scale region, i.e., the quasar host galaxy or a cluster near the quasar (e.g., Weymann et al. 1991); furthermore, a complex AAL without significant variability over decades may trace an outermost remnant of BAL winds fully coupled to the ISM, given the presence of widespread, line-locking signatures in the group-1 quasars. The group-2 quasars, however, have lower systemic redshifts than group-1 quasars, making an identification of C IV AALs impossible from optical spectroscopy. These BAL-acceleration candidates lack or possess shallow Mg II AALs, indicating that AALs tend to be in a relatively high-ionization state, although it is difficult to identify shallow Mg II AAL features from group 2 due to overlapping absorption. Additional insights into BAL acceleration/deceleration and their effects may be gained from X-ray observations, particularly in the context that BAL wind is thought to be associated with the shielding gas.

### 5.2. Implications from Quasar Color

All four quasars have a SED shape consistent with that of red quasars (see Calistro Rivera et al. 2021); however, the group-2 quasars exhibit weak radio emission and are much redder than the group-1 quasars (see Figure 8). If radio emission in group 2 signals a small viewing angle to the jet axis and the group-1 LOS is seen through the edge of a traditional torus, then the group-2 quasars are expected to be bluer than group 1, which is opposite to the observations. As discussed above, the weak radio emission in group 2 is likely a byproduct from BAL–ISM interactions rather than a tracer of low-power jets.

Here, we explore whether the redder color in group 2 is also a consequence of the BAL–ISM interaction. In stark contrast with the variability in rest-frame UV continuum detected in the four quasars, none showed significant variability in the W1 and W2 bands. This difference, along with the partial LOS covering for BAL winds, suggests that the UV continuum variability is likely due to a patchy effect caused by rapid changes in dust composition, distribution, and/or transverse motions during the BAL-acceleration phase. Indeed, the dimming $V$-band brightness in J1259 (see Figure 6) is at least partly caused by the BAL–ISM coupling, a process that can produce rapid changes of the dust/gas in distribution and composition, making in situ dust formation and patchy obscuration possible.

All the four quasars have a SED bump at $\lambda_{\rm rest} \sim 3\ \mu$m, in agreement with the prediction of dusty winds (e.g., Zhang et al. 2014; Gallagher et al. 2015; Calistro Rivera et al. 2021). Importantly, the group-2 quasars have a steeper SED rise at $1\ \mu{\rm m} < \lambda_{\rm rest} < 3\ \mu$m than group-1 quasars, providing further evidence for the correlation between near-IR slope and BAL properties as reported in Zhang et al. (2014), where they speculated that BAL winds are strongly decelerated by interacting with the ISM. Our observations suggest that BAL deceleration may play a more important role than BAL acceleration with respect to controlling the SED shape, perhaps due to stronger in situ dust formation and/or entrainments from an inhomogeneous/clumpy/patchy environment. This result is intriguing and sheds light on the nature of red and blue quasars, especially those with outflows undergoing actual acceleration, as the W3/SDSS-$i$ ratio may change dramatically on short timescales due to changes solely in dust variability along our LOS. Likewise, the conventional classification of radio-loud and radio-quiet quasars would be problematic in such cases (see an alternative tracer of radio-loudness proposed by Klindt et al. 2019). However, the relations between BAL acceleration and UV reddening or brightness are unclear, given that J0136/J1259 become brighter/dimmer in the UV band while both show an increase in UV reddening over the epochs, and that J1238/J1344 become brighter/dimmer in the UV band while both remain generally unchanged in UV reddening. Apart from the inhomogeneous/clumpy/patchy environment, different dust variability behaviors at different wavelengths may also be related to dust composition or in situ dust formation, i.e., the wind–ISM interaction can break dense clouds into diffuse filaments, exposing more dust to quasar UV radiation and hence enhancing IR emission (e.g., Wagner et al. 2013; Hamann et al. 2017).

## 6. Summary

In this work, we select from our sample four LoBAL-acceleration candidates and investigate their physical properties based on multiwavelength, multiepoch observations, aiming to bridge the gap over HiBAL acceleration and gain unique insights into actual quasar feedback. The main observational results and conclusions are summarized below.

1. We identified one compelling (J1344), one strong (J0136), and two tentative cases of LoBAL acceleration, among which J0136 exhibited BAL disappearance in Al III and Mg II (see Section 3).
2. The group 1 (J1344 and J0136) are radio-quiet and exhibit line-locking signatures in C IV AALs, while the group 2 (J1238 and J1259) have red SEDs and weak radio emission with a steep spectral index ($\alpha \sim -1.1$) (see Sections 4.1 and 5.1.2).
3. The BAL–ISM coupling is one of the major avenues for the origin of quasar reddening, patchy obscuration, large-scale AALs, and perhaps weak radio emission (see Section 5.2).

All the four quasars exhibit BAL-acceleration magnitudes larger than the detection upper limits of BAL acceleration derived from Grier et al. (2016), and deserve multiwavelength, follow-up observations, particularly J1259 with its one-sided, off-nuclear [O II] emission nebula. They may provide an ideal laboratory to study the actual feedback processes, such as strong deceleration of BAL winds before traveling out to large scales, the process of BAL winds breaking out of a circumnuclear dust cocoon (e.g., Zhang et al. 2014; Shi et al. 2016; Temple et al. 2019), the origin of giant nebulae from a non-galaxy-cluster environment, the relation between mergers and star formation/quasar activities, and gravitational-wave recoiling SMBHs etc, in the context that LoBALs are representative of young quasars from gas-rich mergers (e.g., Urrutia et al. 2009; Yi et al. 2022).

## Acknowledgments

We thank the anonymous referee for a thorough review and constructive comments, which led to an improved manuscript. We thank for Pu Du, Chen Hu, and Minfeng Gu for stimulating

discussions. We are grateful to Feige Wang, Jingyi Yang, and Xiaohui Fan for assistance with the LBT/MODS observations. W.Y. thanks support from the National Science Foundation of China (NSFC; 11703076). P.B.H. is supported by NSERC grant 2023-05068. Z.Y. is supported by NSFC (12073069) and the Xiaoxiang Scholars Programme of Hunan Normal University. Z.H. acknowledges support from NSFC (12222304 and 12192221). W.Y., J.M.B, and X.B.W. acknowledge the science research grants from the China Manned Space Project with No. CMS-CSST-2021-A06.

This research uses data obtained through the Telescope Access Program (TAP), which has been funded by the National Astronomical Observatories of China, the Chinese Academy of Sciences (the Strategic Priority Research Program "The Emergence of Cosmological Structures" grant No. XDB09000000), and the Special Fund for Astronomy from the Ministry of Finance. Observations obtained with the Hale Telescope at Palomar Observatory were obtained as part of an agreement between the National Astronomical Observatories, the Chinese Academy of Sciences, and the California Institute of Technology. The Hobby–Eberly Telescope (HET) is a joint project of the University of Texas at Austin, the Pennsylvania State University, Ludwig-Maximillians-Universität München, and Georg-August-Universität Göttingen. The Hobby–Eberly Telescope is named in honour of its principal benefactors, William P. Hobby and Robert E. Eberly. The Low-Resolution Spectrograph 2 (LRS-2) was developed and funded by the University of Texas at Austin McDonald Observatory and Department of Astronomy, and by the Pennsylvania State University. We thank the Leibniz-Institut für Astrophysik Potsdam and the Institut für Astrophysik Göttingen for their contributions to the construction of the integral field units. The LBT is an international collaboration among institutions in the United States, Italy and Germany. LBT Corporation partners are: The University of Arizona on behalf of the Arizona Board of Regents; Istituto Nazionale di Astrofisica, Italy; LBT Beteiligungsgesellschaft, Germany, representing the Max-Planck Society, The Leibniz Institute for Astrophysics Potsdam, and Heidelberg University; The Ohio State University, representing OSU, University of Notre Dame, University of Minnesota and University of Virginia. We acknowledge the support of the staff of the Lijiang 2.4 m telescope (LJT). Funding for the telescope has been provided by CAS and the People's Government of Yunnan Province.

## ORCID iDs

Weimin Yi https://orcid.org/0000-0001-9314-0552
P. B. Hall https://orcid.org/0000-0002-1763-5825
Zunli Yuan https://orcid.org/0000-0001-6861-0022
W. N. Brandt https://orcid.org/0000-0002-0167-2453
D. P. Schneider https://orcid.org/0000-0001-7240-7449
Zhicheng He https://orcid.org/0000-0003-3667-1060
Xue-Bing Wu https://orcid.org/0000-0002-7350-6913

## References

Arav, N., Chamberlain, C., Kriss, G. A., et al. 2015, A&A, 577, A37
Arav, N., Liu, G., Xu, X., et al. 2018, ApJ, 857, 60
Aromal, P., Srianand, R., & Petitjean, P. 2021, MNRAS, 504, 5975
Becker, R. H., White, R. L., Gregg, M. D., et al. 2000, ApJ, 538, 72
Blanton, M. R., Bershady, M. A., Abolfathi, B., et al. 2017, AJ, 154, 28
Byun, D., Arav, N., & Hall, P. B. 2022, ApJ, 927, 176
Calistro Rivera, G., Alexander, D. M., Rosario, D. J., et al. 2021, A&A, 649, A102
Capellupo, D. M., Hamann, F., Shields, J. C., Rodríguez Hidalgo, P., & Barlow, T. A. 2011, MNRAS, 413, 908
Chonis, T. S., Hill, G. J., Lee, H., Tuttle, S. E., & Vattiat, B. L. 2014, Proc. SPIE, 9147, 91470A
Costa, T., Rosdahl, J., Sijacki, D., & Haehnelt, M. G. 2018, MNRAS, 473, 4197
Eisenstein, D. J., Weinberg, D. H., Agol, E., et al. 2011, AJ, 142, 72
Fabian, A. C. 2012, ARA&A, 50, 455
Fan, Y.-F., Bai, J.-M., Zhang, J.-J., et al. 2015, RAA, 15, 918
Faucher-Giguère, C.-A., & Quataert, E. 2012, MNRAS, 425, 605
Filiz, Ak N., Brandt, W. N., Hall, P. B., et al. 2013, ApJ, 777, 168
Fynbo, J. P. U., Krogager, J.-K., Venemans, B., et al. 2013, ApJS, 204, 6
Gabel, J. R., Crenshaw, D. M., Kraemer, S. B., et al. 2003, ApJ, 595, 120
Gallagher, S. C., Brandt, W. N., Chartas, G., et al. 2006, ApJ, 644, 709
Gallagher, S. C., Everett, J. E., Abado, M. M., & Keating, S. K. 2015, MNRAS, 451, 2991
Grier, C. J., Brandt, W. N., Hall, P. B., et al. 2016, ApJ, 824, 130
Hall, P. B. 2007, AJ, 133, 1271
Hall, P. B., Sadavoy, S. I., Hutsemekers, D., Everett, J. E., & Rafiee, A. 2007, ApJ, 665, 174
Hamann, F., Herbst, H., Paris, I., & Capellupo, D. 2019, MNRAS, 483, 1808
Hamann, F., Zakamska, N. L., Ross, N., et al. 2017, MNRAS, 464, 3431
He, Z., Liu, G., Wang, T., et al. 2022, SciA, 8, eabk3291
He, Z., Wang, T., Liu, G., Wang, H., Bian, W., Tchernyshyov, K., Mou, G., et al. 2019, NatAs, 3, 265
Hemler, Z. S., Grier, C. J., Brandt, W. N., et al. 2019, ApJ, 872, 21
Hill, G. J., Lee, H., MacQueen, P. J., et al. 2021, AJ, 162, 298
Jester, S., Schneider, D. P., Richards, G. T., et al. 2005, AJ, 130, 873
Joshi, R., Chand, H., Srianand, R., & Majumdar, J. 2014, MNRAS, 442, 862
Joshi, R., Srianand, R., & Chand, H. 2019, ApJ, 871, 43
Klindt, L., Alexander, D. M., Rosario, D. J., Lusso, E., & Fotopoulou, S. 2019, MNRAS, 488, 3109
Kriss, G. A., Mehdipour, M., Kaastra, J. S., et al. 2019, A&A, 621, A12
Leighly, K. M., Dietrich, M., & Barber, S. 2011, ApJ, 728, 94
Leighly, K. M., Terndrup, D. M., & Baron, E. 2014, ApJ, 788, 123
Lu, W.-J., & Lin, Y.-R. 2020, MNRAS, 499, L58
Lyke, B. W., Higley, A. N., McLane, J. N., et al. 2020, ApJS, 250, 8
McConnell, D., Hale, C. L., Lenc, E., et al. 2020, PASA, 37, e048
McGraw, S. M., Brandt, W. N., Grier, C. J., et al. 2017, MNRAS, 469, 3163
Morabito, L. K., Matthews, J. H., Best, P. N., et al. 2019, A&A, 622, A15
Murray, N., Chiang, J., Grossman, S. A., & Voit, G. M. 1995, ApJ, 451, 498
Nair, A., & Vivek, M. 2022, MNRAS, 511, 4946
Nesvadba, N. P. H., Lehnert, M. D., Eisenhauer, F., et al. 2006, ApJ, 650, 693
Panessa, F., Baldi, R. D., Laor, A., et al. 2019, NatAs, 3, 387
Proga, D., Stone, J. M., & Kallman, T. R. 2000, ApJ, 543, 686
Ramsey, L. W., Adams, M. T., Barnes, T. G., et al. 1998, Proc. SPIE, 3352, 34
Rogerson, J. A., Hall, P. B., Rodríguez Hidalgo, P., et al. 2016, MNRAS, 457, 405
Ross, N. P., Graham, M. J., & Calderone, G. 2020, MNRAS, 498, 2339
Roth, N., Kasen, D., Hopkins, P. F., & Quataert, E. 2012, ApJ, 759, 36
Scott, A. E., Brandt, W. N., Behar, E., et al. 2014, ApJ, 797, 105
Shi, X., Zhou, H., Shu, X., et al. 2016, ApJ, 819, 99
Temple, M. J., Banerji, M., & Hewett, P. C. 2019, MNRAS, 487, 2594
Trump, J. R., Hall, P. B., Reichard, T. A., et al. 2006, ApJS, 165, 1
Urrutia, T., Becker, R. H., & White, R. L. 2009, ApJ, 698, 1095
Veilleux, S., Meléndez, M., Tripp, T. M., Hamann, F., & Rupke, D. S. N. 2016, ApJ, 825, 42
Wagner, A. Y., Umemura, M., & Bicknell, G. V. 2013, ApJL, 763, L18
Wang, C.-J., Bai, J.-M., Fan, Y.-F., et al. 2019, RAA, 19, 149
Wang, T., Yang, C., Wang, H., et al. 2015, ApJ, 814, 150
Weymann, R. J., Morris, S. L., Foltz, C. B., et al. 1991, ApJ, 373, 23
Wilson, J. C., Henderson, C. P., Herter, T. L., et al. 2004, Proc. SPIE, 5492, 1295
Xu, X., Zakamska, N. L., Arav, N., et al. 2020, MNRAS, 495, 305
Yi, W., Brandt, W. N., Hall, P. B., et al. 2019, ApJS, 242, 28
Yi, W., Brandt, W. N., Ni, Q., et al. 2022, ApJ, 930, 5
Yi, W., & Timlin, J. 2021, ApJS, 255, 12
York, D. G., Adelman, J., Anderson, J. E., et al. 2000, AJ, 120, 1579
Zakamska, N. L., & Greene, J. E. 2014, MNRAS, 442, 784
Zhang, S., Wang, H., Wang, T., et al. 2014, ApJ, 786, 42